

# **Final Project Report of Stage 1 on the Next Generation model of Bushfires**

Khalid Moinuddin, Duncan Sutherland, Rahul Wadhvani, Sesa Singha Roy,  
Andrew Ooi

**December 2016**

## **Abstract**

Operational models that are used to predict fire behaviour can be implemented easily and rapidly. However, the operational models are only truly valid in the range of experimental conditions used to build the model. This leads to a number of difficulties when using the existing operational models to predict real-world wildfires. Physics-based modelling, that is simulating the fire behaviour from the basic equations of atmospheric fluid flow, combustion, and thermal degradation of fuel materials offers considerable insight into the dynamics of wildfire. However, physics-based simulations are computationally intensive and, at present, can only be applied to small, idealised cases. Nevertheless, the aim of this project is to use physics based models to gain insight into wildfire behaviour and use that insight to improve the current operational models for fire behaviour prediction.

There numerous real-world scenarios that can be investigated using physics based modelling. In this project we focus on three major areas: flow through tree canopies, grassfires, and firebrands. Furthermore, we seek to extend the fundamentals of physics-based modelling by conducting detailed investigations the fluid boundary layer near a rough wall and the fluid boundary layer near a heated vertical wall, both with a view to improving the near-wall modelling employed in Large Eddy Simulation (LES). Each of these subprojects can be considered as largely separate bodies of work within the larger area of physics based modelling. Each subproject will be discussed in detail.

The effect of a tree canopy on the near surface wind speed is investigated using LES with a view to modelling the wind reduction factor (WRF) due to the canopy. The WRF is used in operational fire prediction models such as the McArthur model, to account for the reduction in wind velocity due to a tree canopy. A set of full three-dimensional simulations over idealised rectangular canopies, where the length and leaf area density of the canopy are varied, were conducted. The flow over the canopy is characterised and the potential effects on fire spread of complicated flow structures that develop at the leading and trailing edges are assessed. The simulated wind speed in the fully-developed canopy flow and the wind speed far from canopy region is used to assess the constant WRF modelling approach.

Fires in grasslands are prevalent in Australia, and are relatively simple to model computationally due to the uniform fuel and flat simple terrain. In the present study, the CSIRO grassland experiments are used as validation cases for the physics-based simulations. A parametric study has been conducted where the background windspeed and the grass height have been varied independently. The rate-of-spread (RoS) was found to be linear with windspeed in the parameter range considered. Two simulations were conducted at different heights and correspondingly different bulk density, representing grass which had been cut and left on the ground. The fire in the taller grassland was found to have a higher RoS. Seven simulations were conducted where the bulk density was kept constant as height varied. In these simulations, it was observed that as the grass height increases firefront changes from boundary layer mode to plume mode. Once they are in plume mode higher grass height results in bigger fires, but slower RoS.

The physics of short-range firebrand, or ember, transport is not well understood. The distance and dispersion of the firebrands depends greatly on the turbulent fluid flow which transports the firebrands. The physics-based modelling of firebrand transport is at a preliminary stage. We seek to validate a Lagrangian particle approach for firebrand transport modelling by comparing the results from an experimental firebrand generator with simulations of same scenario. Three particle shapes, cubiform, cylindrical, and disc shaped particles, representing idealised firebrands have been studied. Quantitative features of the landing distribution of the firebrands have been identified. The transport and distribution pattern of uniform, non-combusting cubiform and cylindrical firebrands are compared with a simulated distributions using FDS' default Lagrangian particle approach as well as with improved approach. The results show that the default Lagrangian model gives a good agreement with the experimental data and improved approach yields even better agreement.

Direct Numerical Simulation (DNS) is a numerical technique to faithfully study fluid flows by resolving all the turbulent motions instead of resorting to modelling small-scale turbulence. DNS provides great insight into the physics of flows but is limited to highly idealised and numerically tractable geometries such as channels. Nonetheless, such simulations can be used to gain insight into flows which have relevance to wildfire modelling. Three flows are studied: pressure driven flow over sinusoidal roughness and mixed convective flow (flow driven by both a temperature difference and a pressure gradient).

In the future, the DNS work will contribute to improved turbulence and near-wall modelling used in the physics-based wildfire models. The results of simulations from physics-based wildfire models will in turn improve operational models. We eventually aim to produce models for the WRF, improve knowledge of fire spread in grasslands, and provide a statistical dispersion model of short-range firebrand transport, all of which can be used operationally.

**Keywords:** Wildland fire, WFDS, next generation physics-based modelling, canopy, grassfire, firebrand, turbulent flow

## 1. Introduction

Wildland fires/bushfires are the uncontrolled spread of fires that could occur in areas of the wildland-urban interface areas or wilderness. In recent events, bushfires have encroached on the built environment causing injuries, fatalities and loss of properties and eco-system. The fires caused in these areas can also impact on the viability of living in the surrounding areas. This includes disruption in water supplies due to erosion and contaminants caused by the fires. For such kind of situations, emergency services make considerable use of computer models to predict the behaviour of bushfires. These operational models are capable of providing a range of likely fire scenarios in a timely manner so that appropriate responses can be planned and implemented. This is their great strength, but it also gives rise to one of their limitations. They are inherently limited due to the fact that the data on which they are based cover a limited range of conditions, and we may get results that are unrealistic if we extrapolate beyond the ranges of the models. As Sullivan [1] remarks, empirical models are based on observations, and not on theory. If we are to develop models that accurately predict the rate of spread (RoS) of bushfires over a wide range of conditions, we must ensure that empiricism contributes to its complement, namely rationalism. For this, we turn to the laws of physics that are the unifying principles that permeate this project. Models can be developed drawing on a synthesis of deep knowledge from a wide range of physical science. The laws of physics that govern the rate of spread of bushfires appear to be immutable and universal. They also apply to all of the phenomena that we observe in bushfires. For these reasons, physics-based models are likely

to underpin the next generation of bushfire models. Currently physics-based models are computationally expensive to run. A simulation of a simple grassfire case may take several thousand CPU hours. Therefore these models are not suited to operational use. However, in the future, computational power will improve and numerical modelling technique will improve so that physics based forecasting of fire behaviour will become common. It is in this spirit that the next generation of bush fire models is being developed and utilized under the auspices of Bushfire and Natural Hazard Cooperative Research Centre (BNHCRC).

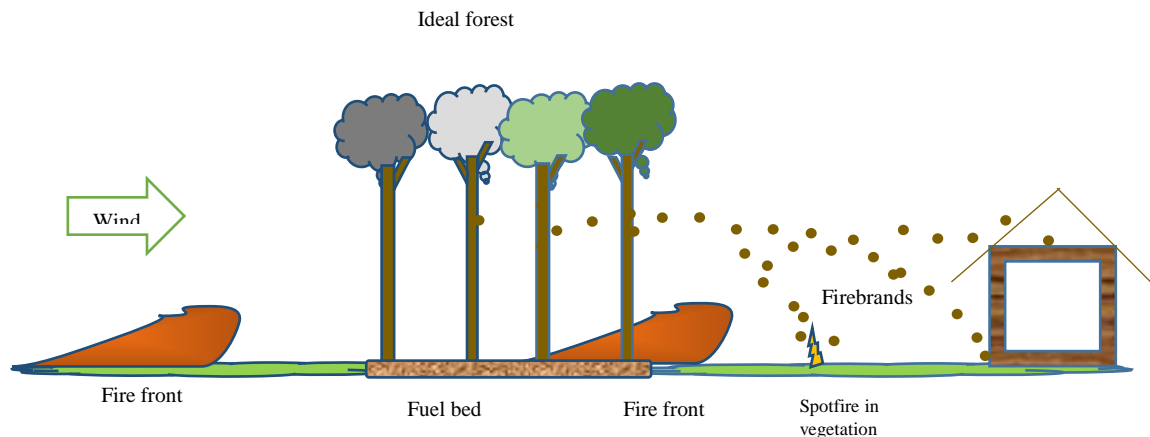


*Figure 1: A schematic of fire spread mechanism in the ideal forest causing spotting in vegetation and house*

*Figure 1* represents an ideal scenario that we are attempting to simulate in unprecedented detail and in the process obtain useful application tools for end-users. To address existing gaps in the mathematical/computational modelling of bushfire dynamics, the scenario shown in *Figure 1* is subdivided into a number of subprojects, covering local windspeed prediction, grassfire spread, effect of surface roughness and temperature, and short-range transport of firebrands.

The rate at which fires spread is overwhelmingly dependent on the wind speed. This is true for fire over open grassland as well as through forests. The velocity profile of the wind within forests is quite different from that over open ground. The dependence of wind speed reduction on forest canopy length and density of vegetation is explored. By comparing wind profiles entering and leaving the canopy we will develop a tool to determine an appropriate wind reduction factor (WRF). We aim to develop a look-up table for operational fighters for appropriate WRF. It is our aim to produce this as the first practical tool which may be utilised from our work.

Grassfires can result in the loss of houses. We are conducting physics-based modelling of grassfire propagation by studying the interaction of the atmosphere with grass, and quantifying the heat, mass and chemical phenomena. The current focus is on the effect of wind speed on the RoS over flat terrain and uniform distribution of vegetation. The results will be compared against the McArthur model [2] and CSIRO model [3]. Another aspect that will be investigated is the effect of grassheight on the rate of spread (RoS). This work will be extended to investigate the effect of slope and fuel inhomogeneity on the RoS. We aim to utilise the model to provide an appraisal of AS3959 [4].

The rate of spread of bushfires is often dominated by embers and firebrands being conveyed ahead of the firefront. We designed and constructed a firebrand generator to accurately quantify how embers disperse. This project will generate experimental data to (a) analyse the dynamics

of short-range spotting and (b) apply/ improve a physics-based submodel to simulate the transport of firebrands. The latter can be further utilised to study the behaviour of firebrand transport under different weather, vegetation and terrain conditions and develop a statistical model for short-range firebrand landing and propensity to cause spotfire. This aspect will be different to lofted long-range firebrand transport being studied by another research team.

The evolution and dynamics of bushfires are very sensitive to the details of the rugged terrain over which they travel. These details range from leaves measured on a scale of a few centimetres, branches measured on the scale of metres to hills and mountains measured on the scale of kilometres. In a computer simulation, it would be impossible to fully simulate the exact physics on all these length scales. These elements of the terrain also obstruct the wind and supply fuel, moisture and heat. Thus, a reliable wall model must capture the aggregate effect of the pertinent physics from all the geometrical length scales, convective heat transfer from earth surface and mass exchange through surface elements. We are working towards a parameterisation of the near-ground flow which includes the effect of the heated earth surface, flows through the canopy (which is inherently rough), and flow above the rough canopy. This will be utilised towards an improvement to wind field generating software such as Windninja [5] to map wind profile (as a function of elevation map, meteorological wind speed and direction) across the simulation domain which will be input conditions for simulation tools.

The key motivation of our work is to improve wildfire modelling so that risks and losses can be reduced. We aim to use results from all these subprojects to develop application tools for fire behaviour analysts and regulators.

## **2. Next generation physics based model**

In our bid to develop a next generation physic-based model of bushfires we have deemed it desirable to build on existing computational platform. We endeavour to extend and refine the Fire Dynamics Simulator (FDS) developed by NIST[6] for building fire and its sister model for wildfire Wildland-Urban Interface Fire Dynamics Simulator (WFDS). FDS is fundamentally a finite difference approximation to the equations of fluid motion. That is, the computational domain is discretised into cells or control volumes. The set of partial differential equations for the conservation of mass, momentum and energy for a Newtonian fluid are solved by the FDS model.

The FDS/ WFDS solves numerically a form of Navier-Stokes equation appropriate for low Mach number, thermally-driven flow (Mach number  $< 0.3$ ) with an emphasis on smoke and heat transport from fires. Under the auspices of the BNHCRC, next generation fire modelling team made a number of improvements to the FDS/WFDS model. These are presented below:

### **2.1. Improved methods of modelling turbulence**

In attempting to conduct simulations of grassfire, similar to Mell et al. [7], we found the results would depend strongly on the chosen spatial resolution. In part, this is because the flows encountered in bushfires are highly turbulent. LES only resolves the large scale fluid motion and models all subgrid scale turbulence. Therefore, care must be taken to ensure that the subgrid scale turbulence models do not change with the grid itself. In order to overcome this difficulty we developed an explicit filtering scheme and verified the scheme using two well-known benchmark cases: fluid flows over a backward-facing step and buoyancy driven cavity flow (Sarwar [8]).

## 2.2. Implementation of canopy profile

Typically, a canopy is modelled (example Mueller et al [9]) as a source of aerodynamic drag. That is, an additional body force term is added to the momentum equations where the canopy is present. The aerodynamic drag term is:

$$f_{b,i} = \chi(x, y, z) \frac{\rho}{2} c_D \alpha(z) u_i u_i, \quad (1)$$

where  $\chi(x, y, z)$  is one if  $(x, y, z)$  is inside the rectangular canopy region and zero otherwise. The fluid density is denoted by  $\rho$  and the drag coefficient is  $c_D$ .  $\alpha(z)$  is the Leaf Area Density (LAD) of the canopy, which is assumed to only vary with height.  $u_i$  is the  $i^{th}$  component of velocity (that is  $i$  represents either the  $x, y$ , or  $z$  directions.) LAD is the amount of volume occupied by the frontal area of the vegetation. Profiles of LAD can be measured by scanning LiDAR or can be modelled with simplified approximations. We implemented two methods of prescribing the LAD. Firstly, the LAD may be read from a data file. This is useful if LiDAR scans of a forest exist, however, no attempt has yet been made to simulate a real forest. The second method is to model the LAD as a product of an indicator function and a function of height alone. That is,

$$a(x, y, z) = a(z) \text{ if } x_0 < x < x_1, y_0 < y < y_1, \text{ and } 0 < z < h, \quad (2)$$

where  $(x_0, y_0)$  are the coordinates of the origin of a rectangular canopy and  $x_1 - x_0$  and  $y_1 - y_0$  are the lengths of the canopy in the  $x$  and  $y$  directions respectively. The height of the canopy is  $h$ . Multiple rectangular canopies can be specified, which allows the representation of complicated heterogeneous canopies. Typically canopies exhibit strong variation with height, for example, many forests have more leaves at the top of the canopy than the bottom. As a simple model of many forest profiles, such as those measured by (Moon et al [10], Shaw et al [11] or Amiro [12]) a Gaussian profile is used. That is,

$$a(z) = A e^{(-\sigma(z-h_0/h)^2)} + B \quad (3)$$

where  $B$  is a constant shift in LAD, representing the contribution by the tree trunks to LAD,  $A+B$  is the maximum LAD,  $\sigma$  sets the width of the LAD distribution, and  $h_0$  is the height of the maximum LAD. By carefully choosing the parameter values, all profiles measured by [10] can be approximated.

For more complicated distributions of LAD, such as the bimodal distribution observed by Amiro [12], it is possible to fit a superposition of Gaussians to the data. The implementation of the canopy model in FDS permits overlapping canopies, which are treated as a superposition of the canopy profiles.

## 2.3. Improved methods of firebrand transport

While verifying the validity of the default Lagrangian particle model of FDS for the transport of non-combustible firebrands (NCFB) of different shapes (for details of the verification study refer to section 3.4), it is observed that the existing Lagrangian particle model under-predicts the spatial distribution of NCFB. To correct this issue, we used a correction in the drag coefficient to incorporate the effect of sphericity. Sphericity ( $\psi$ ) is a measure of how spherical (round) an object is. It is defined as the ratio of the surface area of a sphere (with the same volume as of the given particle) ( $S_{sph=part}$ ) to the surface area of the particle ( $S_{part}$ ):

$$\psi = \frac{S_{sph=part}}{S_{part}} = \frac{\pi^{\frac{1}{3}}(6V_p)^{\frac{2}{3}}}{A_p} \quad (4)$$

where,  $V_p$ ,  $A_p$  are particle volume and surface area.

We use two different correction models for drag coefficient: Equation (5) (Haider et al [13]) and Equation (6) (Sommerfeld et al [14]).

$$C_{D,Haider} = \frac{24}{Re_D} (1 + ARe_D^B) + \frac{C}{1 + \frac{D}{Re_D}} \quad (5)$$

Where,

$$A = \exp(2.3288 - 6.4581\psi + 2.4486\psi^2)$$

$$B = 0.0964 + 0.5565\psi$$

$$C = \exp(4.905 - 13.8944\psi + 18.4222\psi^2 - 10.2599\psi^3)$$

$$D = \exp(1.4681 + 12.2584\psi - 20.7322\psi^2 + 15.8855\psi^3)$$

$$C_{D,Hölzler} = \frac{8}{Re_D} \frac{1}{\sqrt{\psi_{\perp}}} + \frac{16}{Re_D} \frac{1}{\sqrt{\psi}} + \frac{3}{\sqrt{Re_D}} \frac{1}{\psi^{0.75}} + 0.42 10^{0.4(-\log(\psi))^{0.2}} \frac{1}{\psi_{\perp}} \quad (6)$$

Where,  $\psi_{\perp}$  denotes cross-wise sphericity which is the ratio between the cross-sectional area of the volume equivalent sphere and the projected cross-sectional area of the considered particle perpendicular to the flow.

## 2.4. Improved methods of convective heat transfer to surface

The convective heat transfer model currently used for LES is the overall heat transfer models for boundary layers across the whole layer. Inconsistent with the LES models for momentum equations, heat transfer near solid surface should be calculated using eddy diffusivity rather than the overall heat transfer coefficient. A new model is developed using the eddy diffusivity concept to determine the convective heat transfer coefficients at the surface ( Moinuddin and Li [15]).

## 3. Physics-based modelling results

### 3.1. Sub-Canopy wind flow

The rate-of-spread of the boundary of a wildfire depends on the wind speed. The presence of a tree canopy will act as an aerodynamic drag force and reduce the wind speed. In, for example, the McArthur [16] model, this effect is modelled by using a wind-reduction factor (WRF). The WRF is often defined as the ratio of the wind speed at 10 m height, in the open far from any canopies, to the wind speed at 2 m height within the canopy as given in Moon, et al. [10]. The sub-canopy height of 2 m is selected to represent the mid-flame height, which is believed to be the most relevant wind spread to characterise the fire spread.

Currently, to model the WRF, fire behaviour analysts use a rule-of-thumb based on the measurements of McArthur [16]. A recent and extensive field study conducted by Moon, et al. [10] has demonstrated that the wind reduction factor can vary over a wind range, and depends on forest type, mean wind speed in a canopy free region, and atmospheric stability. Moon, et al. [10] has proposed a statistical model that could be used operationally to estimate the WRF.

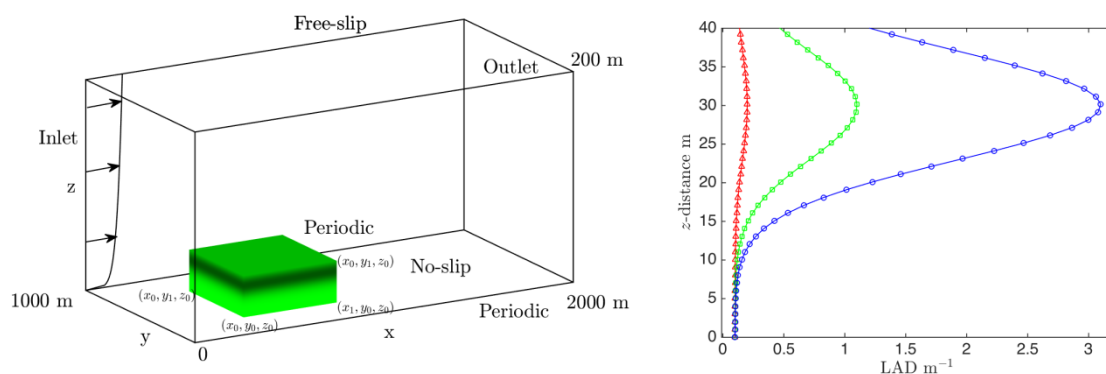
The sub-canopy wind velocity has received considerable attention in the fluid mechanics and meteorological literature. For example refer to Harman and Finnigan [17], Wilson and Shaw [18]. Effectively, these works attempt to parameterise the mean wind speed inside the canopy. Most efforts to develop a simple model of wind velocity start with the model of Inoue [19]. For a fully developed sub-canopy wind far from any canopy edges the velocity is well modelled by a balance between the aerodynamic drag due to the canopy and the transfer of momentum in the fluid due to the turbulence.

LES is quickly becoming the preferred tool to investigate complicated atmospheric flows. Simulations of sub-canopy winds have been successfully conducted, for example, Mueller, et al. [9] and Cassiani, et al. [20]. In this study, FDS' LES submodel is used to simulate wind flow over an idealised rectangular-shaped tree canopy. In particular, we seek to characterise the development of wind speed over, within, and downstream of the canopy. We then seek to appraise a simple model of the WRF based on the model of Inoue [19].

### 3.1.1. Methodology

The literature on LES for atmospheric and canopy simulations is extensive. In particular, studies by Bou-Zeid, et al. [21] show that LES can reproduce experimentally observed velocity profiles and higher order turbulence statistics. Therefore this simulation approach is appropriate for the present study. For a complete discussion of LES methods refer to Pope [22].

The domain considered for the first set of simulations and an outline of the LAD is sketched in *Figure 2*. We conduct six simulations of flow over canopies with varying LAD and canopy length between 100 and 900 m. The LAD profiles are selected to be representative of a variety of terrestrial tree canopies Amiro [23]. The region from the ground to approximately 15 m represents the drag exerted by the trunks of the trees (and any intermediate forest storey). The region from 15 m to the top of the tree represents the leafy crown. The height of the crown 40 m is selected to be representative of typical forest heights throughout Australia (which are in the range of 20 m to 60 m). The primary variation in the LAD of a forest is within the tree crown, the most-dense LAD considered here is representative of a dense Spruce forest Amiro [23], and the least dense LAD is representative of a Eucalyptus regrowth forest Moon, et al. [10]. The intermediate value of LAD is selected simply as a convenient value between the two extremes.



(a) Domain of simulations showing the coordinates, mean inlet profile and the canopy location within the domain. The 500 m canopy is shown.

(b) The profiles of LA as it varies with height within the canopy. Red (triangles) most sparse canopy, green (squares) intermediate canopy, blue (circles) dense canopy.

*Figure 2: Simulation conditions*

### 3.1.2. Results

#### *General features of the flow: detailed examination of the a particular case*

To begin characterising the flow field over the tree canopies, we firstly examine case 500 m long canopy with  $\max(LAD) = 3.1$  in detail. The time-averaged streamlines are lines instantly tangent to the mean flow, over the canopy, within the canopy, near the edges and near the exit region of the canopy are plotted in *Figure 3*.

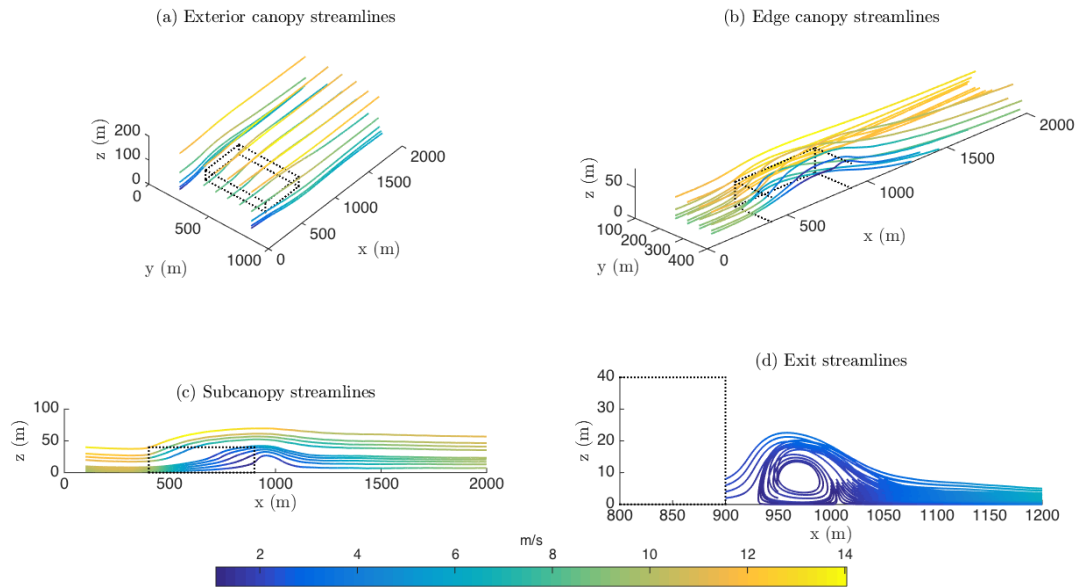


*Figure 3: Streamlines within the various flow regimes. The streamlines have been constructed from the time averaged data and coloured by the velocity magnitude. (a) the streamlines around the canopy, (b) the streamlines through the canopy, (c) the edge streamlines, (d) streamlines in the recirculation region showing the presence of a large, but slowly rotating vortex*

Far upstream of the canopy, near the inlet, the imposed wind profile is a realistic Atmospheric Surface Layer (ASL). Near the leading edge of the canopy, an impact region is observed:  $\bar{u}$ -velocity profile decreases rapidly. Correspondingly, by continuity, the spanwise, or lateral,  $\bar{v}$ -velocity and the vertical  $\bar{w}$ -velocity increase. The streamlines are pushed upwards in this region and they are also pushed towards the lateral edges of the canopy.

Near the downstream boundary of the canopy, a recirculation and reattachment region may develop. A large slowly rotating vortex structure can form. This recirculation region was first investigated by Cassiani, et al. [20]. Far downstream of the canopy the velocity profile starts to recover to the upstream profile.

#### *The effect of canopy length and LAD on the centreline flow*

The centreline  $\bar{u}$ -velocity profiles of the other canopy cases are plotted in *Figure 4*. In this case, the trunk space is sparse relative to the tree crowns, and a strong secondary maximum of velocity is seen in the impact region. This secondary maximum decays with distance along the canopy. Similar trunk space maxima have been observed by Dupont, et al. [24] and Wilson and Shaw [18].

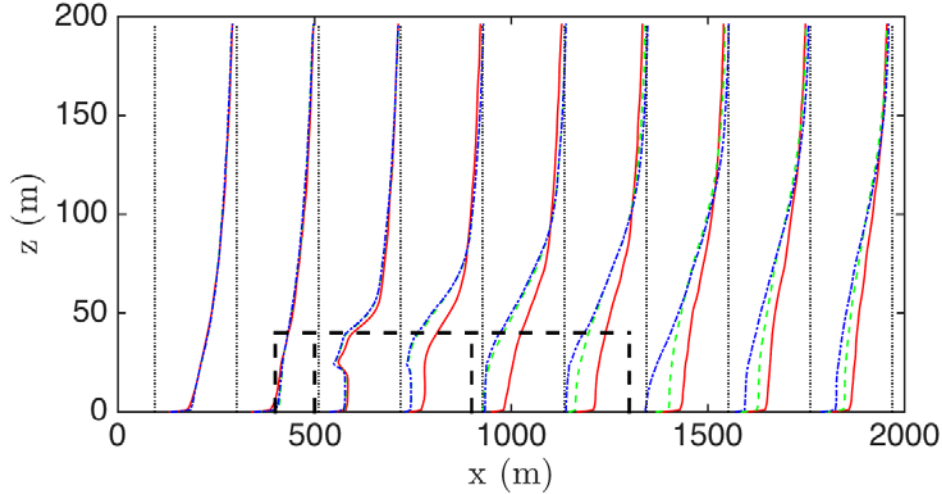


Figure 4: Centreline average stream wise velocity profiles along the 100 m (red solid), 500 m (green dashed), and 900 m (blue dotted) canopies, with fixed LAD profile. The flow develops almost identically within the canopies.

Eventually the velocity profile within the canopy will become self-similar and this is called fully developed canopy flow. For these cases, the flow does not quite fully develop before exiting the canopy. The flow above the canopy also develops and forms a wake downstream of the canopy. It is possible to use a periodic geometry, like that used by Mueller, et al. [9], to study the fully developed canopy and above canopy velocity profiles, however, the impact region and exit regions then do not exist.

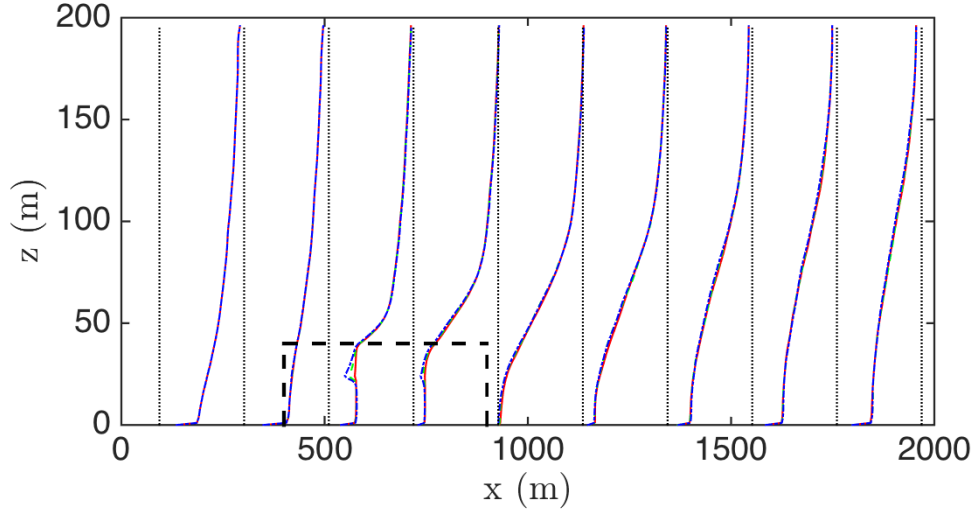


Figure 5: Variation in the average streamwise velocity profiles along 500 m canopies with variation in LAD. Red(solid):  $\max(\text{LAD}) = 0.2$ , green (dashed): 1.1, blue (dotted) 3.1. Note only the minor differences in the leafy crown region.

The  $\bar{u}$ -velocity profiles along the centre line of the domain varying with LAD are shown in Figure 5. Only minor differences are observable in the tree crown part of the canopy as the flow develops in the impact region. This is consistent with our modelling approach where only the leafy crown of the tree changes. Importantly, this result demonstrates that apart from near the upstream canopy edge, the leafy tree crowns do not affect the overall velocity profile. In the fully developed region, the main contribution to the drag is apparently due to the trunks and

large branches. Therefore, the fully developed sub-canopy wind will not be significantly affected by the burning away of the leafy crowns.

Harman and Finnigan [17] use the model of Inoue [19] for sub-canopy velocity, which with appropriate normalisation to ensure continuity of velocity at the top of the canopy is

$$\bar{u}_c(z) = \bar{u}_a(h) \exp\left(\frac{(z-h)c_D\bar{a}}{2\beta^2}\right). \quad (7)$$

This model assumes that within a canopy of infinite size, the fluid momentum is then governed by two terms, the momentum flux transport due to turbulence (Reynolds stress) and the drag exerted by the canopy. The equations for  $\bar{u}_c(z)$  and  $\bar{u}_a(h)$  form a model for the wind profile above and within the canopy respectively.

The model compares well to the fully developed sub-canopy winds observed in the Tumbarumba forest and the Duke forest over a wide range of atmospheric stabilities (Harman and Finnigan [17]).

This modelling approach assumes the velocity profile is independent of the x-location within the canopy. The horizontal distance along the canopy has significant effect on the velocity profile. *Figure 4* shows that for the 900 m canopy case the profiles become roughly independent of x-location after about 600 m into the canopy, this is approximately 15 canopy heights, which is consistent with the measurements of Dupont, et al. [24]. Hence, the model cannot be expected to capture the profiles near the upstream edge of the canopy. However, the model should reproduce the simulated velocity profile near the downstream edge of the canopy. Importantly, the model should provide a lower bound on the sub-canopy wind velocity within canopies of finite size.

To test the model we plot (*Figure 6*) the centreline velocity profiles at all x-locations within the canopy region, and compare to the simple model. The average velocity profile over the whole canopy, and the average velocity profile over the last 400 m of the canopy are also plotted for comparison. The average profile over the whole canopy shows a prominent trunk-space maximum which, as expected, is not captured by the simple model. However, the model compares qualitatively well, inside the canopy, to the average over the last 400 m of the canopy where the profile is most developed. There is a significant discrepancy in the profile above the canopy. In the above canopy region there is a growing internal boundary layer which does not fully develop and hence the model is poor in this region.

To compute a wind-reduction factor from this model is straightforward. We adopt a  $p=1/7$ -powerlaw to model the wind profile far from the canopy because it does not require estimation of roughness and displacement lengths like a logarithmic model. The relative wind speed in the canopy is then

$$RWS(z) = \frac{u_r(z/z_r)^{\frac{1}{7}}}{\bar{u}_c}. \quad (8)$$

A range of wind reduction factors can then be estimated by considering the inverse of this ratio. The model gives a range of WRF  $\sim 2$  at the top of the canopy to WRF  $\sim 19$  at the bottom of the canopy. This is consistent with Moon, et al. [10] who found the WRF varied between 2.3 to 14.4 across the canopies studied. The slight discrepancy may be due to the choice of  $p=1/7$ . This value is chosen because it provides a good model of the wind speed over bare soil Morvan, et al. [25]. However,  $p$  varies depending on the atmospheric stability and the nature of the surface (Peterson and Hennessey Jr [26]) and a different choice of  $p$  may be appropriate to

match the modelled WRF with the data of Moon, et al. [10]. Therefore  $p$  should be considered a model parameter, along with  $\alpha_t$ ,  $u_r$  and  $z_r$ .

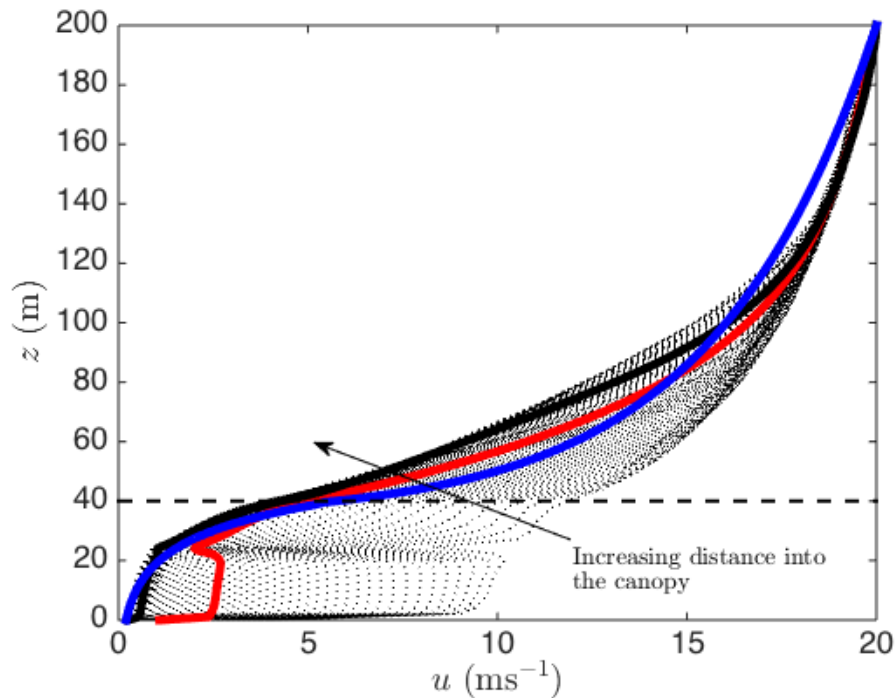


Figure 6: The centreline velocity profiles within the canopy (black dotted) for case 900 m canopy. The red line is the average of all the centreline velocity profiles, the black (solid) line is the average centreline velocity in most developed part of the canopy flow, and the blue line is the model of Harman and Finnigan [17]. The thick black dashed line indicates the top of the canopy.

### 3.1.3. Further works

The heat generated by bushfires gives rise to buoyancy-driven plumes that interacts with the wind. Because a plume entrains fluid from every direction, the recirculation region is unlikely to persist as a fire exits the canopy. However, the complicated recirculation structure may affect the transport of firebrands. The wake structures, large regions of slow moving fluid, which are shed from the canopy may impact fire behaviour for a great distance downstream. Further simulations are required to understand the effect of the canopy on the rate-of-spread, and further work is required to extend the study to a realistic, irregularly shaped, inhomogeneous tree canopy.

## 3.2 Grassfire propagation

### 3.2.1. Pyrolysis model validation

There are two thermal degradation sub-models within the physics-based model to simulate the pyrolysis of the fuel – Linear [27] and Arrhenius [6] and to apprise them we investigated thermal degradation of Lucerne hay. Lucerne hay is one of the animal feedstock crops grown in Victoria, Australia. Lucerne hay is selected to minimise the effect of site variation and increase reproducibility of experimental work. The thermal degradation of Lucerne hay is carried out using a Mettler Toledo thermogravimetric analyser (TGA) TGA/DSC in an inert atmosphere of nitrogen from 30-900 °C. The Lucerne hay is divided into two sections: leaf section (the upper section of hay consisting of blade, leaf, and seeds) and stem section (the

bottom section of hay containing stem, and nodes). The samples are conditioned at 27°C and relative humidity of 50% for more than 36h before testing in TGA. The samples are labelled as LuS, LuL and LuM representing Lucerne stem section, Lucerne leaf section and Lucerne mixture which is 50-50 wt.% mixture of Lucerne stem and leaf respectively.

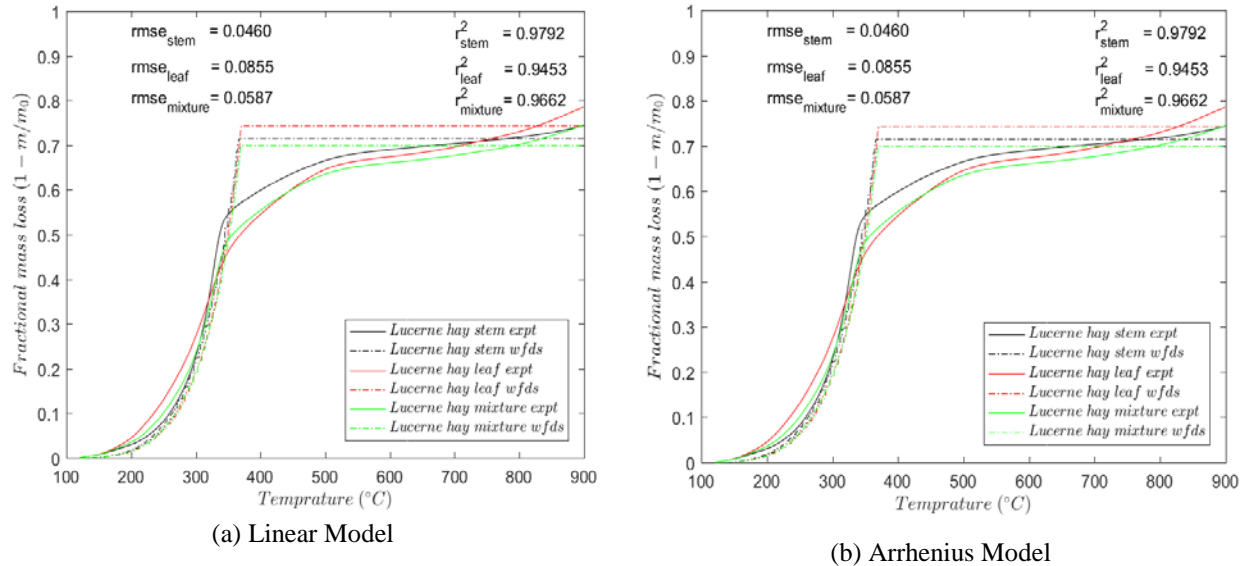


Figure 7: Fraction mass loss observed for experimental and simulated models for Lucerne hay at constant heating rate of 20 K/min

Figure 7 (a) shows the comparison between the experimental fractional mass loss observed in TGA and simulated fractional mass loss using WFDS with the linear model. Figure 7 (b) shows a similar comparison using the Arrhenius model. It is quite visible from Figure 7 that the linear model simulates the thermal degradation section 220-360 °C accurately. The Arrhenius model does a poor job due to use of a single best-fit model for a complicated multi-step thermal degradation reaction. The computational time required to simulate using linear model is  $\sim 1/10^{\text{th}}$  of the Arrhenius model.

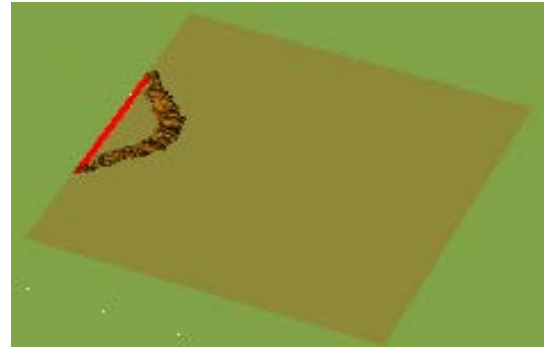
Hence, for a large-scale bushfire physics-based simulation, it is acceptable to utilise the linear model which requires using TGA to estimate the mass loss curve to obtain the thermal degradation section, DSC to estimate the heat of pyrolysis, and a hot disc analyser to measure heat capacity.

### 3.2.2. Fire spread model validation

Australian grassland fires were investigated by CSIRO researchers in Australia Cheney, et al. [28] due to the simplicity afforded by relatively flat terrain and homogeneous fuel. Also, there is a number of experimental data available for validation. The rate of spread was considered a key factor that was studied in relation to these experiments. The Australian grassland experiment was conducted on a 104 m x 108 m plot 4.6 m/s wind was measured at 2 m above the grass surface blowing left to right. Ignition was started by two field workers at the centre of the left-hand-side. The workers then walked in opposite directions and took over 56 seconds to complete the line ignition. Figure 8 shows the experimental snapshots of the above mentioned experiment and physics based simulation.



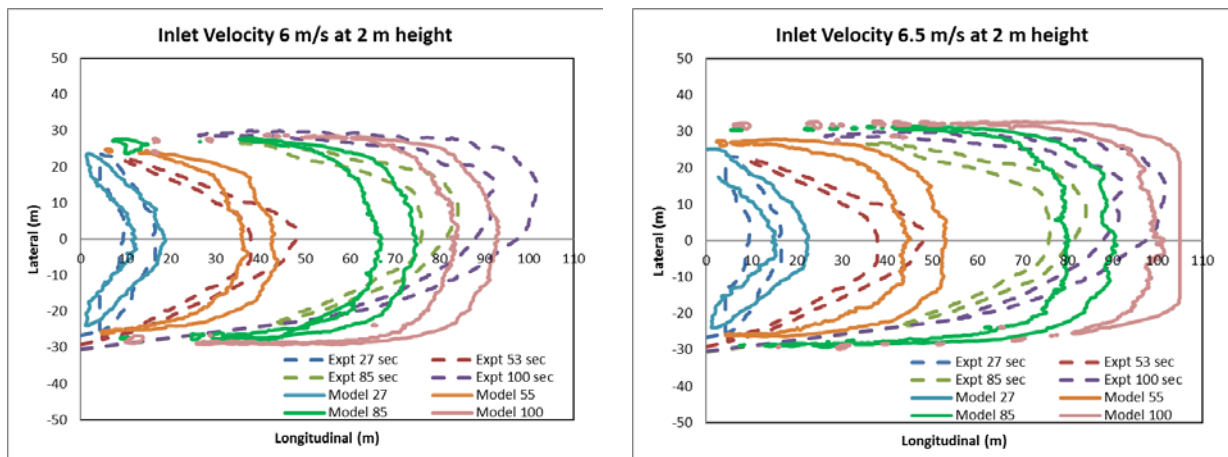
(a)



(b)

Figure 8: (a) Burning of Australian grassland and (b) physics-based simulation

The choice of the size of the grid (cell) in a mesh is one of the first and most important decisions one must make when conducting a quantitative simulation. The choice of grid size can affect the results. To be meaningful, numerical simulation results need to be sufficiently resolved so that the results do not change with the grid. In this case, the simulation is said to be grid-converged. For the grid convergence study, the RoS results of the same case simulation with different grid sizes are compared and found with 250mm grid cells grid converged solutions are observed for grassfire with linear thermal degradation model.



(a) 6 m/s at 2m height at inlet

(b) 6.5 m/s at 2m height at inlet

Figure 9: Model validation: fire propagation. Solid lines physics-based model result. and dashed line experimental results.

In Figure 9 the fire perimeter propagation from experimental study and two simulations (obtained using 250 mm grid) are presented. One simulation was conducted with wind velocity 6 m/s at 2 m height at the inlet and the other had 6.5 m/s wind velocity at the same location. The fire spread occurs from left to right. The fire perimeters are plotted 27 s, 53 s, 85 s, and 100 s after the start of ignition. It can be observed that fire line progression is reasonably well predicted by the physics-based model.

### 3.2.3. Effect of Wind velocity

When wind speed is varied, the physics-based model has predicted faster fire spread rate than the Mk V (McArthur) model ([2], but slower than the CSIRO model ([3] as shown in Figure 10. However, the numerical results predict an unusually high rate of spread (ROS) when  $U_{10}$  is

3 m/s. Furthermore, the numerical result is extraordinarily linear (though CSIRO model is also linear beyond 6 m/s  $U_{10}$ ). Both aspects need to be further analysed. CSIRO model demonstrates two modes of propagations: boundary layer mode and plume mode (these are well known and discussed by Apte, et al. [29]). At low  $U_{10}$  (5 m/s and below) the firefront is in the plume mode and beyond that the firefront is inclined by higher wind velocity resulting them into boundary layer mode.

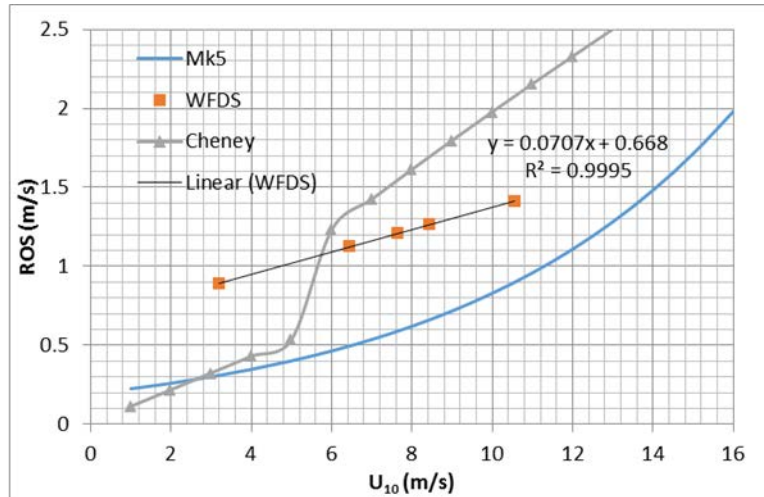


Figure 10: Effect of wind velocity on rate of spread (ROS)

### 3.2.4. Effect of grass height

Preliminary studies with simulations with two different grass heights (250mm and 160 mm) are presented in Figure 11. It should be noted that vegetation load (tonne/ha) is the same for both cases. This means in Figure 11(b) case, original 250mm high grass was mowed down to 160mm and the cut grass was still lying on the grassland. This obviously changed the bulk

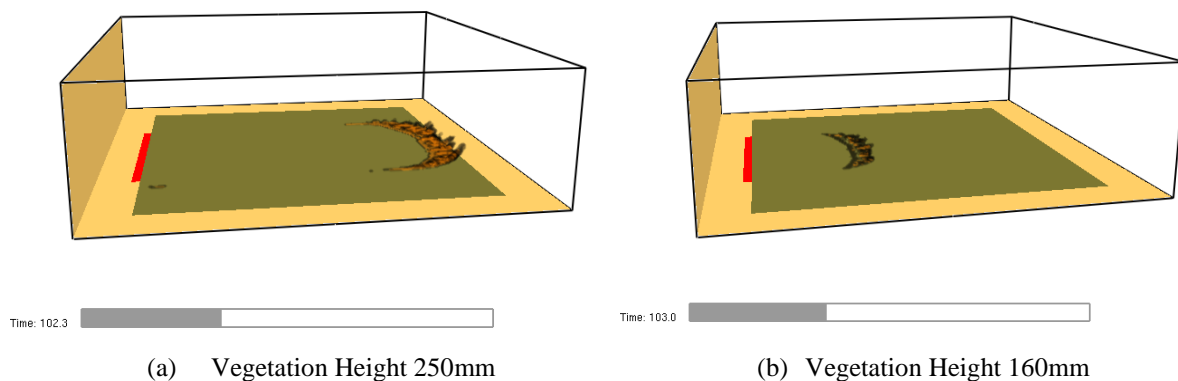
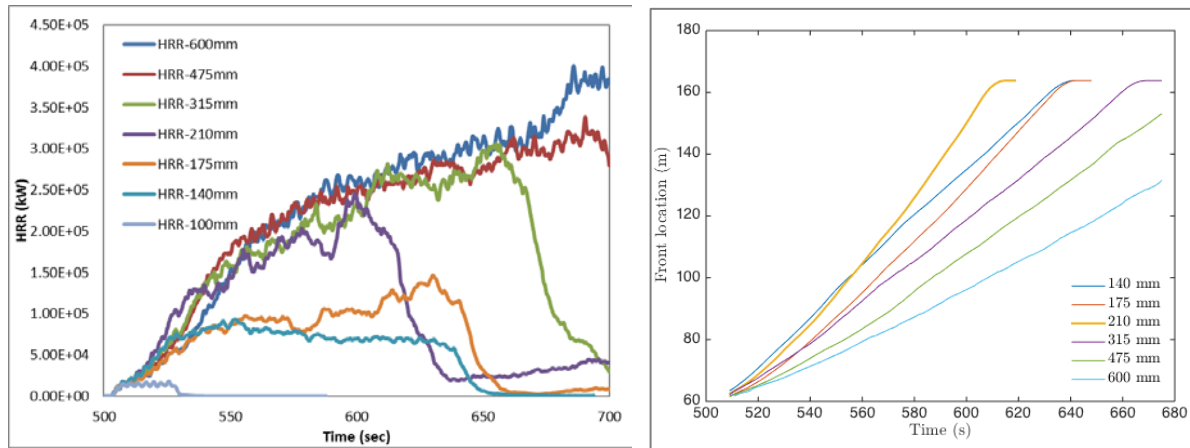


Figure 11: Effect of vegetation height

density i.e. Case b (Figure 11(b)) had higher bulk density. The results in Figure 9 shows that fire propagated at a higher rate of spread for the Case a (Figure 11(a)), where grass height is higher and bulk density is lower. Lower bulk density promotes higher surface temperatures leading to greater pyrolysis of the grass as per Equation (7.3). This further leads to bigger fire (as seen in Figure 11) and quicker progression.

A second set of simulations was carried out with seven different grass heights (100, 140, 175, 210, 315, 475 and 600 mm). Here vegetation load is varied proportional to the grass height and bulk density is maintained constant i.e. no grass was considered to be mowed.



(a) Heat release rate

(b) Location of fire fronts

Figure 12: Effect of vegetation height. (a) HRR and (b) locations of fire fronts as function of time. 140 and 175mm cases are in boundary layer mode of propagation. 600, 475, 315 and 210mm cases in plume mode of propagation. In the plume mode, increasing grass height in these simulations leads to a decrease in rate of spread.

The HRR vs time curves are presented for all seven cases in Figure 12(a). 100 mm case shows fire dies down soon. Four cases: 600, 475, 315 and 210mm have the same trend. On the other hand two cases: 140 and 175mm shows another trend. It also demonstrates two modes of propagations: boundary layer mode and plume mode (Apte, et al. [29]). During the initial settling period the all cases are in boundary layer mode (where firefront is highly influenced by the wind flow within the boundary layer), once it reaches certain HRR threshold (big enough to overcome wind pressure) it switches to the plume mode. 140mm case did not reach that threshold – so it remained in boundary layer mode. 175 mm remained in boundary layer mode for most of the duration and then eventually switches to a plume mode.

It appears that as the grassheight increases, due higher amount of fuels available, more fuel pyrolysis and fire sizes grow bigger leading to firefront overcoming boundary layer effect. As a result RoS changes to a plume mode and results in slower RoS as the grassheight increases. 600, 475, 315 and 210mm cases are truly in the plume mode of propagation. In the boundary layer mode, firefront is inclined towards the ground ie virgin fuel ahead leading to receiving higher convective heat. As a result virgin fuel ahead of the firefront pyrolyses quickly and RoS is fast.

In Figure 12(b) locations of fire fronts as function of time are present (the slope of each curve represents RoS). Leaving aside 140 and 175 mm cases, a clear trend is observed for the plume mode propagation (210 mm case onwards): spread rate decreases with height.

### 3.3 Tree and Canopy fire

For tree burning simulations, experiments conducted at National Institute of Standard and Technology (NIST) in which Douglas-fir was the selected tree species are considered [27]. During the NIST experiments, 2.25m high trees were mounted on custom stands and allowed to dry. The trees were ignited using a custom igniter: circular natural gas burners with a specific heat release rate of 30 kW. The mass was measured and the mass loss rate calculated taking

into consideration the moisture content in the samples. We have used two thermal degradation sub-models within the physics-based model to simulate the tree burning experiments – WFDS (Linear) (Mell, et al. [27], Mell, et al. [7]) and FDS (simplified Arrhenius) ( McGrattan, et al. [30]). Both software packages otherwise have the same fluid flow, turbulence, continuity, pressure, energy, radiative heat transfer and combustion models. The aim of this study is twofold: one we seek numerically converged results, which were elusive in the original study Moinuddin, et al. [31] and secondly we appraise the linear and Arrhenius models for thermal degradation.

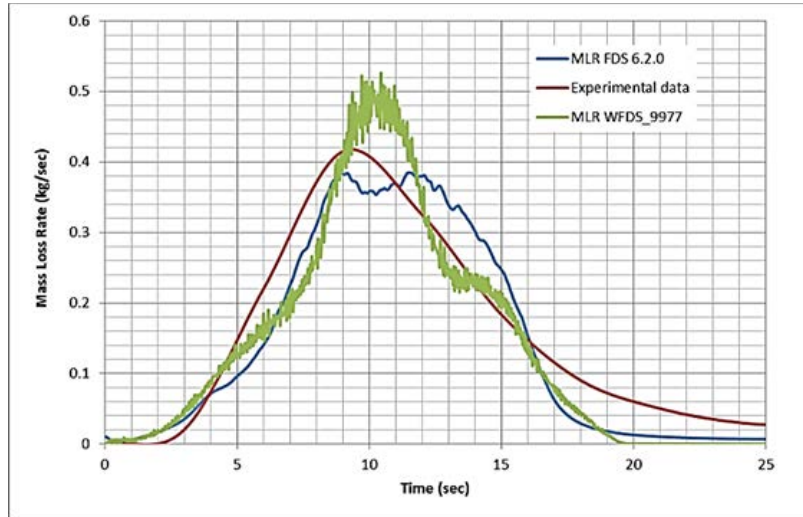


Figure 13: MLR results comparison with experimental data [2]

### 3.3.2. Results

First of all, the grid convergence study, the Mass Loss Rate (MLR) and Heat Release Rate (HRR) results of the same case simulation with different grid sizes are compared. To simulate a 2.25m high Douglas fir tree, we selected 75 mm, 50 mm and 37.5 mm grid cells for WFDS (Linear) and 100 mm, 50 mm and 37.5 mm grid cells for FDS (simplified Arrhenius). Comparison of MLR and HRR results for the three simulations with each model shows that convergence is deemed to be obtained with 50 mm grid for both models.

When the MLR results of two (FDS and WFDS) grid converged simulations (where 50 mm grid cells are used) are compared with the experimental result in Figure 13. It can be observed that the area under the MLR curve are approximately the same. The averaged total mass loss from nine experiments was 3.62 kg. It is exactly the same for FDS (simplified Arrhenius) and within 1.5% while the simulation is conducted with WFDS (Linear).

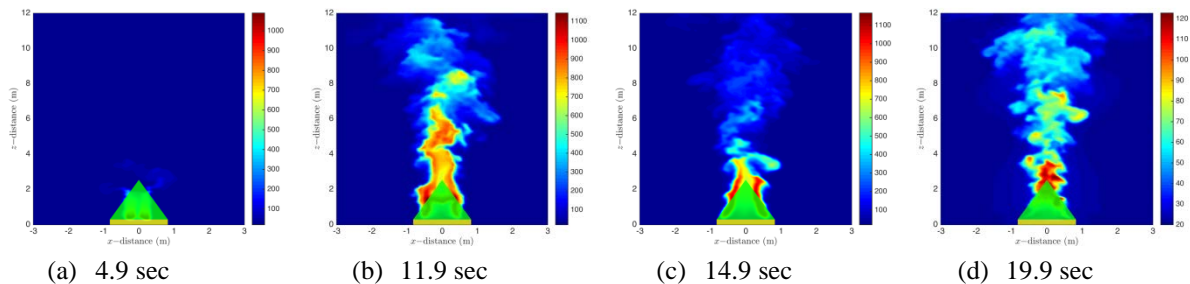


Figure 14: Graphical representation of Douglas fir tree burns simulation. The results from the WFDS simulation is depicted to show the gas-phase temperature at various instances of time after ignition.

Figure 14 shows snapshots of simulations of a 2.25 m tall tree using WFDS' companion graphical output software Smokeview from Forney [32]. Figures represent temperature slices to show the gas-phase temperature at various instances of time after ignition.

With successful quantitative simulation of 2.25m Douglas Fir tree along with achieving numerical convergence, we now attempt to model a scenario where forest floor fire interacts with tree canopy. We have used WFDS (Linear) due to its lesser computational resource requirement. As FDS (simplified Arrhenius) needs 100,000 particles of each type of vegetation parts per unit volume, it needs enormous computational resources to model a number of trees.

We have modelled a forest of Douglas Fir trees sitting on a grassland. This is absolutely a hypothetical scenario (it may not be practical, though possibly it can be a model of a plantation) to assess whether fire can progress from the surface to the crown. The simulation domain is 96 m long, 8 m wide and 10 m high as shown in Figure 15. The inlet is prescribed as power law (1/7) ABL (atmospheric boundary layer) with a wind speed of 3 m/s at 2 m. Two lateral edges are modelled as periodic.

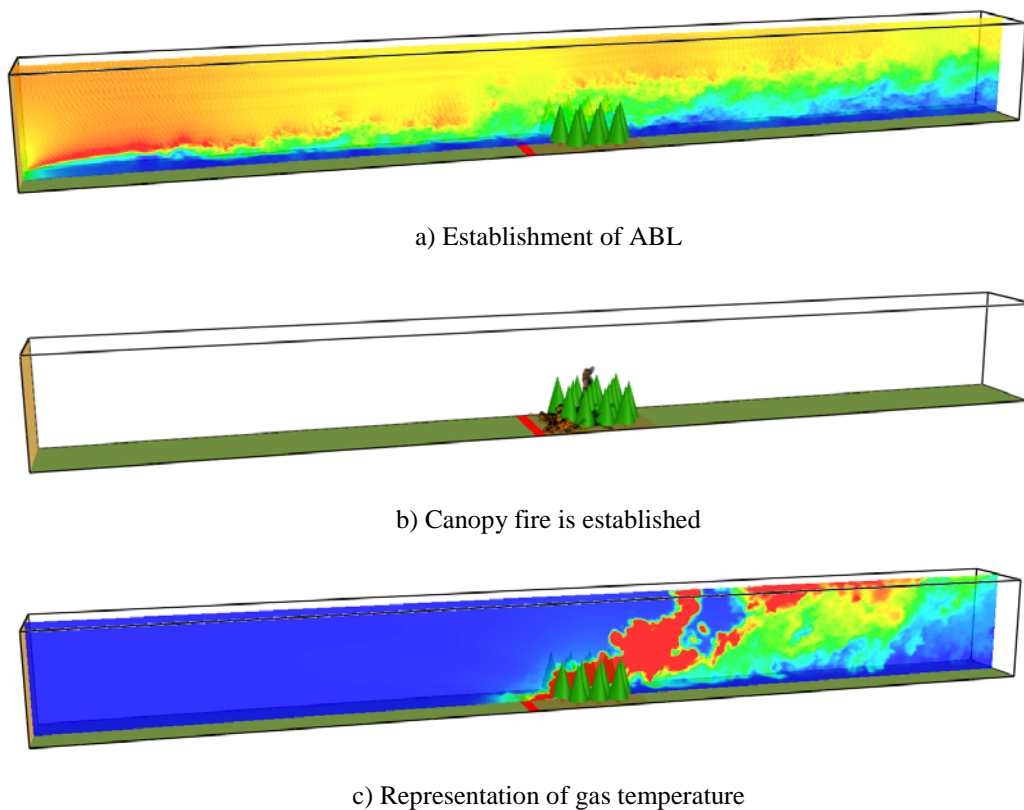


Figure 15: Graphical representation of surface fire-crown interaction simulation.

The outlet and top of the domain are modelled as open. 44 m from the inlet in the longitudinal direction, the burnable grass plot (12 m long) is placed so that there is another ~40m subdomain downstream of the plot before reaching an open outlet. 100 mm x 100 mm x 100 mm grids are used throughout. While this is coarser than required for grid convergence for the burning of the trees, previous results/discussions in Section 3.2.2 show that it is adequate to simulate grassfire spread. With coarser grid ignition time to crown fire from grassfire appears to be underestimated by few seconds only. On the other hand, while surface fuel was used as forest litter (instead of grass), coarser grid overestimated ignition time to crown fire. However, for

both cases, in the short period after ignition, a 100 mm grid is found to be sufficient to reproduce the correct MLR and HRR. The aim of this study, however, is to simply assess model's ability to predict the transition from surface to crown fire. If this transition occurs with a coarse resolution, then the same transition can be expected with a finer grid simulation. The finer grid will be necessary for any quantitative study on the transition.

Four longitudinal columns of Douglas Fir trees were modelled. The crown was approximated as cones and the trunk as cylinders. For simplicity, the crowns are modelled only as needles with  $2.2 \text{ kg/m}^3$  bulk density. Alternately columns had three and four trees in a staggered fashion. The columns are 2 m apart and within the column, the trees are also 2 m apart. Prior to an actual simulation of fire line spread, a precursor simulation was carried out to map ABL above the grassland within the simulation domain. An established ABL can be observed in *Figure 15(a)* (before it impacts on the canopy). Established canopy fire is shown with  $500 \text{ kW/m}^2$  heat release rate per unit area in *Figure 15(b)* and gas-phase temperature at that instance is represented in *Figure 15(c)*.

### 3.3.3. Summary

This study shows that a wildfire can be quantitatively simulated using a mixture of fuels and the rise in temperature at various distances from the fire front can be predicted. By changing the properties of fuels, simulation of native Australian vegetation can be attempted. In the future, similar simulations will lead to greater understanding of the transition of surface fires to crown fires and could be used to construct threshold models of crown fire transition. The largest drawback of physics-based simulations remains the large computational time due to the extremely fine grid sizes required. However, a simple linear parameterization of thermal degradation can be used to reduce some of the computational effort.

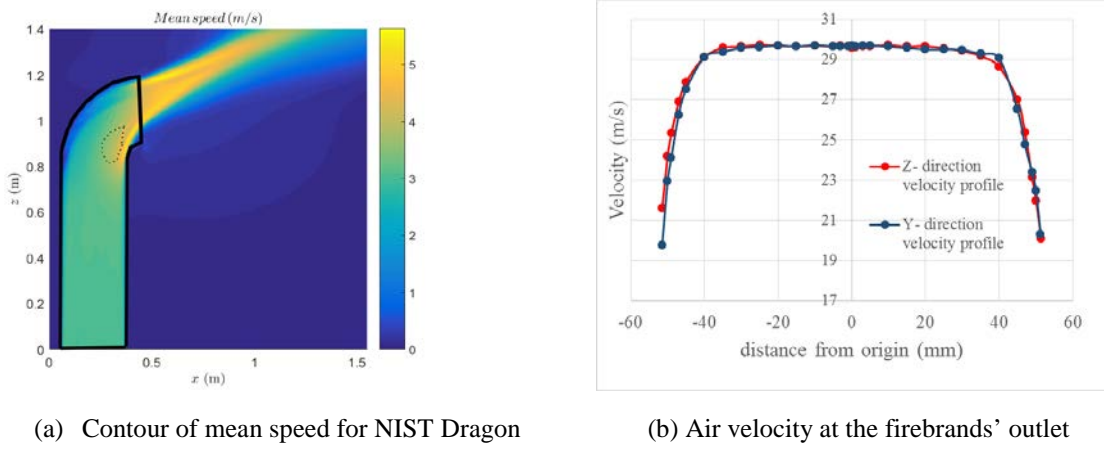
## 3.4 Firebrand transport

Firebrands generated by bushfires are the cause of spot fires which increase the overall rate of spread of the fire. Firebrands comprise a range of components such as species bark, twigs, and leaves. The flow of firebrands in the wind has not been studied in detail, and the existing physics-based model to describe the flow and aerodynamics of firebrand does not incorporate the effect of shapes and sizes of the firebrand. Currently, within FDS the model used is the Lagrangian particle model. In this model the trajectory of the individual particle is tracked in the fluid flow, however, it is applicable only when the particles are small in comparison to the scale of flow. This component of the project is motivated by the need to devise comprehensive models of the dispersion of embers and firebrands, and their propensity to ignite vegetation. This objective is achieved by characterising the key physical and chemical properties of firebrands and embers generated by a range of Australian flora and determining their aerodynamic properties.

### 3.4.1. The design and construction of a firebrand generator

For credible computer-generated models, the results of the model must be validated against experimental data. Hence, a firebrand generator is designed and constructed so that the distribution of firebrands can be modelled and measured. Previously NIST has developed a firebrand generator (Manzello, et al. [33], Manzello and Suzuki [34], dubbed a 'Firebrand Dragon', to study the interaction of firebrands with buildings, but the NIST Firebrand Dragon suffers from non-uniform flow profile due to sudden  $90^\circ$  bend before the firebrands' release. This issue is termed as Dean's vortex (Dean [35]) and highlighted in the contour of NIST Dragon in *Figure 16 (a)*. Similar observations of non-uniformity for this pipe shape observed in the literature (Mohanarangam, et al. [36], [37], Sun, et al. [38], Chu and Yu [39]). Hence,

the distributions of the firebrands and air velocity at the dragon's mouth are highly non-uniform. Thus, we have designed a firebrand generator involving two co-axial pipes which produce a uniform air velocity at the mouth as shown in *Figure 16 (b), (c) and (d)*.



(a) Contour of mean speed for NIST Dragon

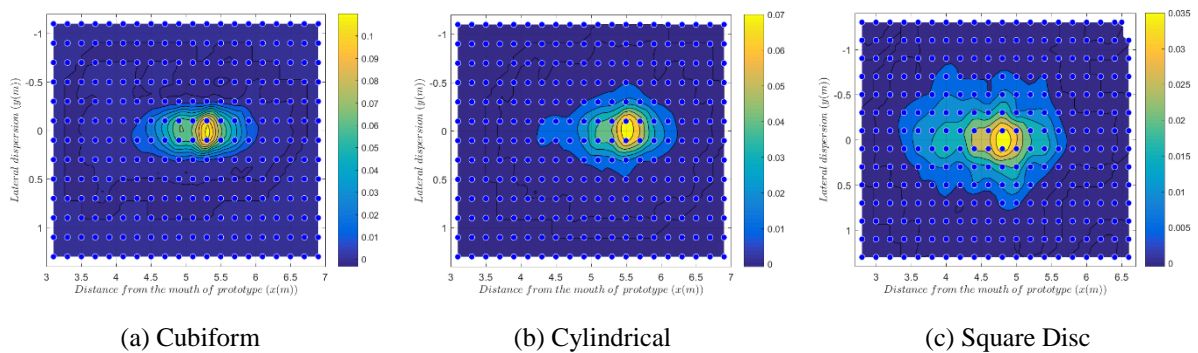
(b) Air velocity at the firebrands' outlet



(c) Firebrand generator prototype

Figure 16: Firebrand Generator prototype and velocity distribution

In the present phase of the project, we are comparing the experimental results with the existing computational Lagrangian particle model in FDS. We also measure the velocity of firebrands and their scattering patterns. The effect of passive firebrands' shape (cubiform, cylindrical and square disc shape non-burning firebrand particles) on the transport of firebrand using firebrand generator prototype is studied. The particles after falling on a firebrand collecting pad bounce and collide with each other, so to obtain accurate statistical distribution video analysis of scattering are carried out, and the first impact location is measured. The average scattering plots of their first impact on the pads shown in *Figure 17*. A tail is observed closer to the firebrand generator in the particle distribution shown in *Figure 17 (a) and (b)* for cubiform and cylindrical firebrands, which is not very prominent for the square disc as seen in *Figure 17(c)*.



(a) Cubiform

(b) Cylindrical

(c) Square Disc

Figure 17: Contour plot of the first impact distribution of non-burning firebrands

Regarding the distance travelled the order is: Cubiform > Cylindrical > Square disc. We can see more span wise scattering in the case of square disc firebrands compared to other two types. Regarding the span wise scattering, the order is: Square Disc > Cylindrical > Cubiform.

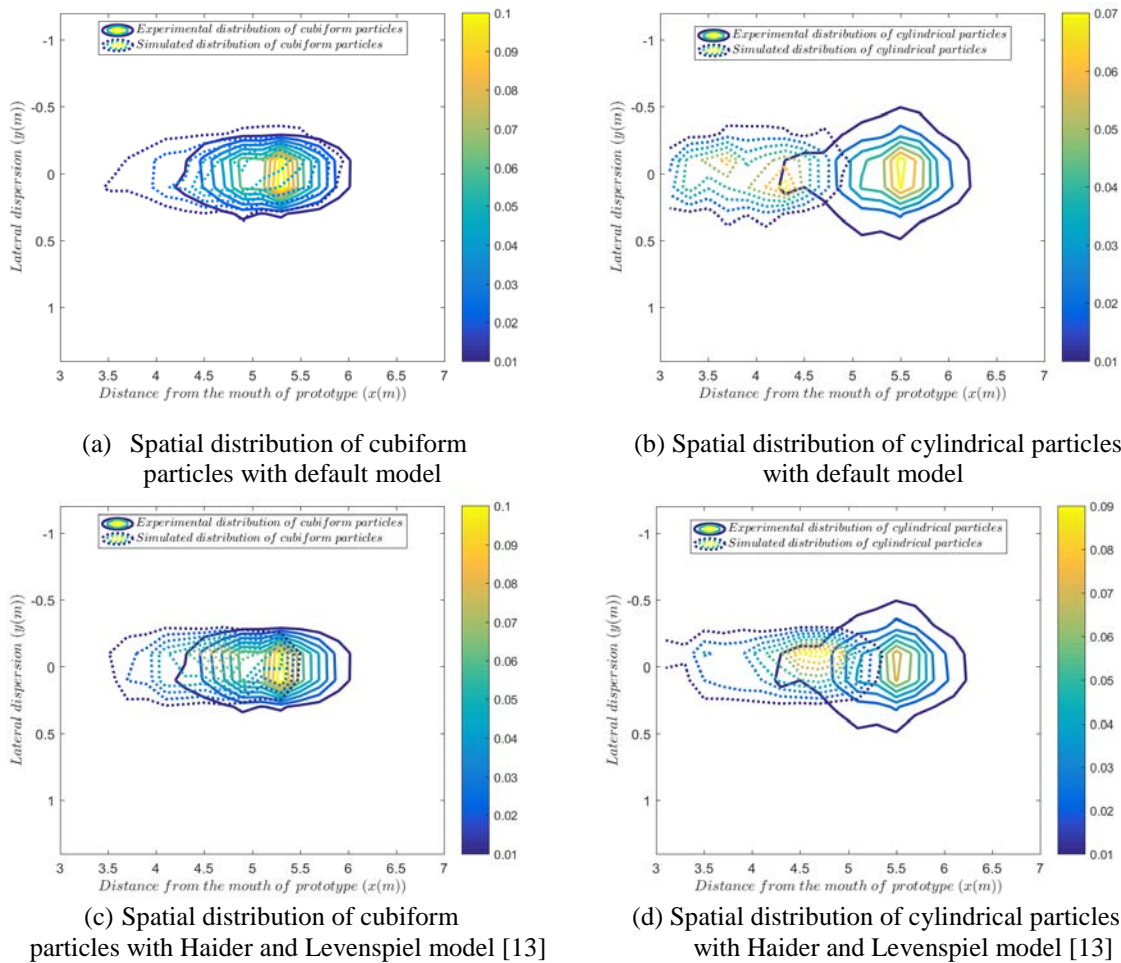


Figure 18: Spatial distribution of cubiform and cylindrical particles with default FDS models and with Haider and Levenspiel models [13]

Simulations of above experiments are carried out in FDS for cubiform and cylindrical particles. Figure 18(a) shows the comparison between the simulated contour of cubiform with the default and modified drag models (detailed in section 2.1.11 and 2.2.3). Figure 18(b) shows a similar comparison for cylindrical particles with the default and modified drag models.

The spatial distribution of cylindrical particles with the default model was significantly under-predicted (Figure 18(b) and (d)) and is corrected with the Haider and Levenspiel model (discussed in section 2.2.3). The new model has very little impact on the cubiform particles (Figure 18(a) and (c))

### 3.5 Flow over topographical features using Direct Numerical Simulation

A detailed understanding of wind flow behaviour is required to model fire propagation effectively as it is primarily driven by the wind. Wind flow behaviour depends on a range of factors including the topography, earth surface temperature and other ambient weather conditions. We studied two idealised problems with Direct Numerical Simulation (DNS). The primary difference between DNS and LES is that all relevant turbulent scales are resolved using DNS, there are no additional models apart from the conservation of momentum, energy, and

mass. This allows great insight into the physics of turbulent flows. However, only small problems in highly regularised geometries and Reynolds number (a dimensionless measure of turbulence) flows are possible. We studied flow of sinusoidally rough surfaces which is an idealisation of topography and the flow over a vertical heated surface. We aim to develop simple wall functions which can be implemented into the physics-based model of wildfire spread.

### 3.5.1. The simulation of turbulent flows over rough surface

Wind speed profile (the variation in wind speed with respect to distance from the ground) is strongly influenced by topography. For atmospheric flow, the topography is often modelled as a rough surface which promotes the generation of turbulence and offers greater resistance to the wind flow near the earth's surface. As a result, the topography affects the rate of spread of a fire and therefore its intensity. Higher wind speeds tilt the flames forward to pre-heat the fuel ahead of the fire and push the fire along increasing the rate of spread. Understanding how wind speed changes as it passes through grasslands or forests is, therefore, crucial to developing better fire behaviour predictions in support of firefighting agencies.

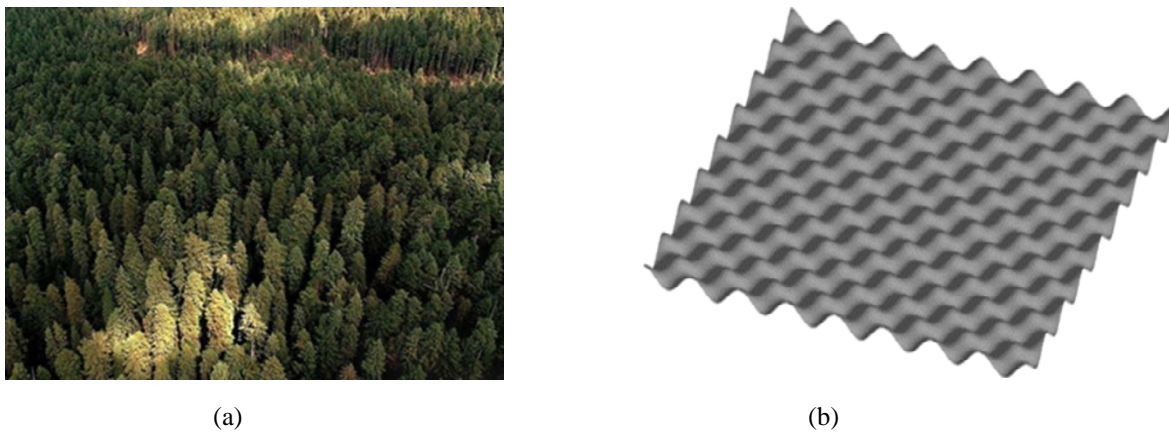


*Figure 19: A forest (a) can be treated as a rough surface, but for modelling purposes that can be idealised as shown in (b). In the limit the undulations can become needle-like so that they simulate the behaviour of trees.*

Computing the exact physics of turbulent fluctuating flow over grasslands, forests and canopies is a very expensive and resource-intensive process. Scientists need to use complicated mathematical models and state of the art sophisticated computational algorithms many thousands of CPU hours on the largest supercomputers. It is not feasible for practitioners to resort to powerful computers in order to account for roughness in order to calculate the profile of the wind as it flows over forests and urban landscapes. Instead, practitioners seek some simple mathematical parameterization that captures the main dynamics of velocity fluctuations near the rough wall. For example, parameterisations of the near wall velocity over forests are required for numerical weather prediction.

Due to the fact that the turbulent flow over real-world rough surfaces can get overly complex and mask the pertinent physics, we have chosen to concentrate our efforts in understanding the flow over an idealised sinusoidal surface. *Figure 19* compares a forest to the idealised surface used in this study.

The velocity profile of the wind flowing over smooth surfaces is very well established, but for practical applications, we need to know the velocity profile over rough surfaces. Roughness is characterised by the solidity ( $\Lambda$ ) of the roughness (MacDonald, et al. [40]). Generally speaking,

solidity is the frontal area of the roughness elements which are exposed to the wind. If the solidity is low the roughness is called sparse, and if the solidity is high, the roughness is dense.

The sparse and dense regimes of roughness were investigated using direct numerical simulations of the flow over three-dimensional sinusoidal roughness. The minimal span channel technique, recently used by Chung, et al. [41] for rough-wall flows, was used.

The dense regime of roughness was found to occur when the solidity was greater than approximately 0.15. In this regime, the velocity fluctuations within the roughness elements decreased, although were not negligible even for the densest case. The limit as solidity tends to infinity appears to correspond to a smooth wall in which the wall was located at the crest of the elements, and second order statistics did show the dense roughness cases were tending towards this limit.

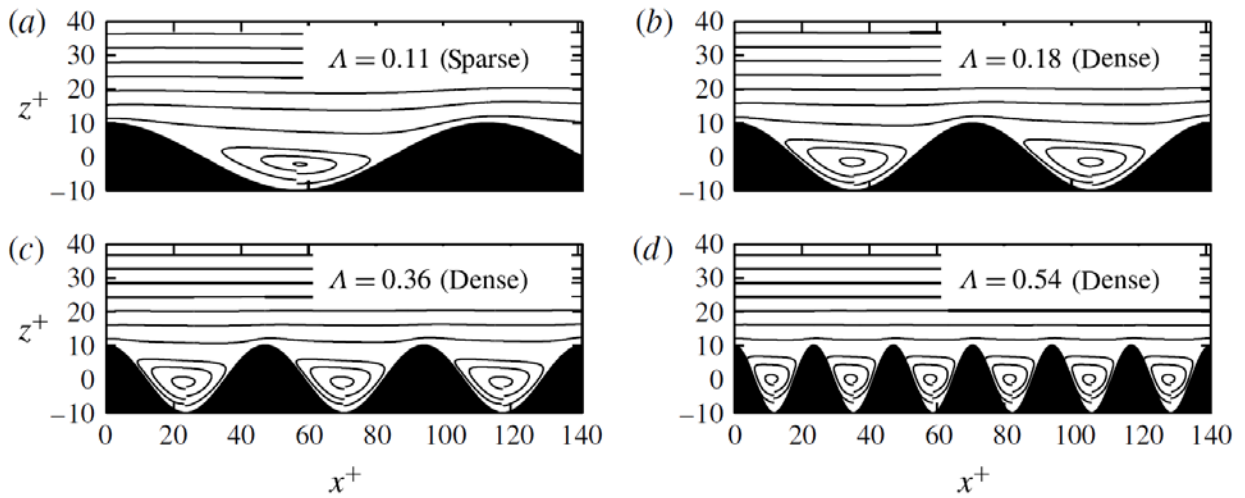


Figure 20: Mean streamlines over roughness of various solidity, in the stream wise-wall-normal plane. Flow is in (a) sparse and (b–d) dense regimes.

Conceptual models of the dense regime of roughness often describe stable vortices within the roughness elements, with high-speed fluid skimming over the top of the roughness. The sparse regime, meanwhile, is described by a much smaller recirculation zone with respect to the roughness crest, with the separation point being closer to the reattachment point. In order to assess the veracity of these descriptions, the mean streamlines are shown in *Figure 20* for both sparse and dense roughness. All four sets of streamlines show an almost identical flow pattern, with the recirculation region appearing similar in terms of the roughness wavelength. The area of flow recirculation,  $A_R$ , does scale with solidity according to  $A_R/A_T \approx 0.18 \log(\Lambda) + 0.9$ , where  $A_T$  is the total area occupied by fluid below the roughness crest; however, there does not appear to be a distinct change in flow structure between the sparse (*Figure 20a*) and dense (*Figure 20b–d*) regimes. It is clear that these qualitative descriptions of roughness are not adequate on their own to indicate the existence of the dense regime or to explain why a slightly different flow pattern results in a reduction in the roughness function.

*Figure 21(a)* shows the mean velocity profile for the smooth wall ( $\Lambda=0$ ) and a sparse regime case ( $\Lambda=0.11$ ). It can be observed that roughness reduces the velocity profile. On the other hand, from *Figure 21(b)*, it can be observed that beyond wall unit  $z^+ > 20$ , velocity profile over dense rough wall rises above the velocity profile over a sparse rough wall and it increases with  $\Lambda$ .

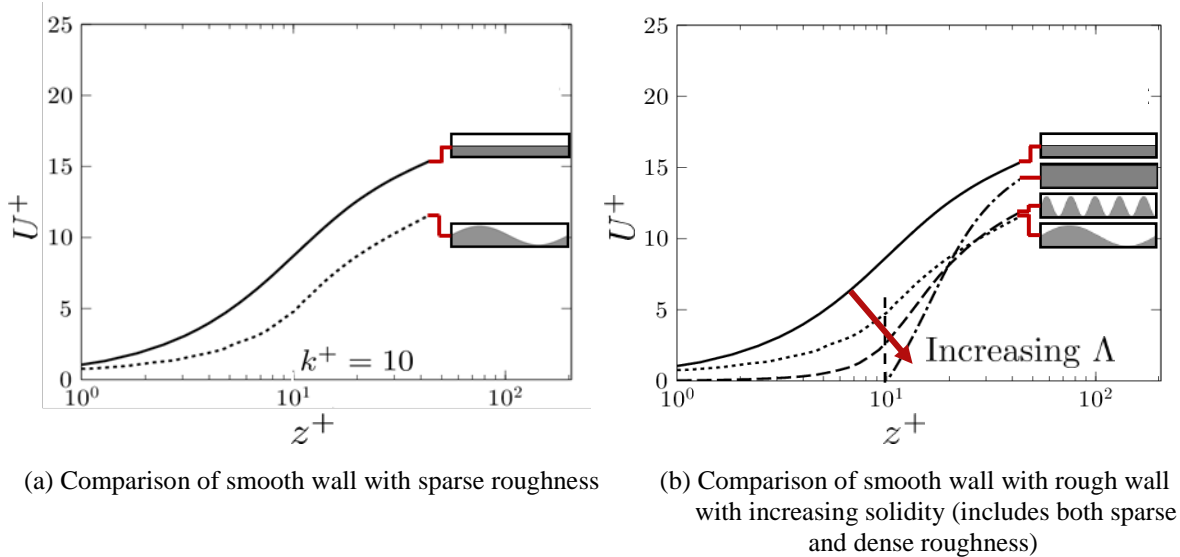


Figure 21: Mean velocity profile

An analysis of the mean momentum balance enabled the roughness function to be decomposed into two contributions. This revealed that the primary reason for the reduction in the roughness function that is seen in the dense regime is due to the reduction in Reynolds shear stress above the roughness elements. The near-wall cycle, located at  $z^+ \sim 15$  for a smooth-wall flow, is pushed up above the roughness elements. As the solidity increases the location of the near wall cycle also increases. In the infinite solidity limit, the rough wall effectively becomes a smooth wall located at the roughness height  $k^+$ , and therefore the near-wall cycle is located at  $z^+ \sim k^+$  plus 15 wall units. Spectral analysis indicates that the dense regime gradually reduces energy in the long streamwise length scales that reside close to the roughness elements. As the density increases, the long streamwise length scales are increasingly damped and the near-wall cycle is pushed up away from the wall.

From the above study, simple equations can be derived for the difference in the velocity profiles as a function of roughness. By choosing the appropriate dimensions of the surface tree-like objects, the velocity profile can be accurately calculated. This can be useful for atmospheric boundary layer modelling.

### 3.5.2. Airflow over heated surface

When the surface of the earth is heated, the profiles of air velocity and temperature adjacent to the surface are changed. The logarithmic law of the wall is typically used to describe the mean velocity of the flow in the near wall region where the production of turbulence due to a shear flow is much larger than the production of turbulence due to buoyant effects. The law of the wall allows the shear stress to be specified as a boundary condition and allows the boundary layer velocity profile to be modelled in LES.

There are many examples of fluid flow over heated vertical (and inclined) surfaces, particularly in bushfire scenarios. For example, accurate predictions are required of the behaviour of fires as they interact with buildings and structures at the bushfire-urban interface.

A well-established theory by Monin-Obukhov to predict the near surface velocity and temperature profiles over a horizontal surface exists, but it is not clear if the same theory applies to an inclined or vertical surface. The aim of this fundamental science study is to see whether an idealised law, in the boundary layer regime of the flow, much like Monin-Obukhov theory exists for a vertical surface. If the same law exists for both horizontal and vertical surfaces, it

can be assumed the law would be the same for all inclined surfaces. Similarly, if different laws exist for horizontal and vertical surfaces then there will be a dependence on slope angle for inclined surfaces.

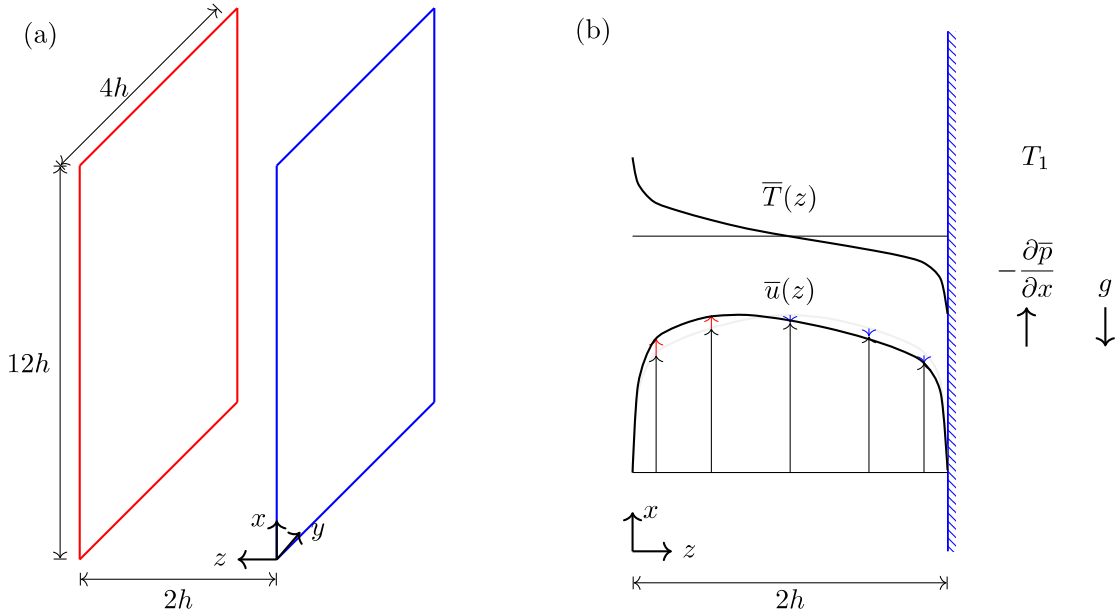


Figure 22: Sketch showing the vertical channel geometry, and the mean profiles of velocity and temperature. The effect of aiding (red arrows) flow and opposing (blue arrows) flow is also shown.

This work is of great significance to meteorology and fire prediction. Many physical scenarios involve simulating wind and temperature fields over the complicated terrain. In these simulations, so-called wall models are used to parameterise the near surface behaviour. Accurately representing the near-wall behaviour of the air velocity and temperature fields near non-horizontal surfaces will improve the quality of the overall simulations. Wall models that may be derived from this study could be applied to numerical weather prediction, high-resolution wind modelling, and smoke transport modelling.

In this study, numerical solution of the equations that govern mixed convection flow between two differentially heated vertical plates are conducted at low Reynolds numbers (quantifying the pressure-driven flow), and seven Richardson (denoted  $|h/L|$  numbers (a parameter representing the balance between buoyancy and pressure-driven flow). There are two flow regimes. One regime is called aiding flow, where buoyancy acts in the same direction as the pressure-driven flow. The second regime is called opposing flow where buoyancy acts in the opposite direction to the flow. These are analogous to an unstable, and stable atmosphere respectively. A schematic of the flow setup is shown in *Figure 22*.

For the aiding cases, the mean velocity shows a marked departure from the traditional logarithmic boundary layer profile in *Figure 23*. However, this effect is not seen in the opposing cases and the profiles exhibit collapse to the neutral (no buoyancy) profile. Neither the aiding nor opposing mean temperature profiles collapse well to the canonical profile. For opposing flow cases the velocity fluctuations and Reynolds stress show significant increases from the traditional profiles. However, for aiding flow cases the opposite occurs, the velocity fluctuations and Reynolds stress decrease from the neutral profiles. Temperature fluctuations decrease from the neutral value in the aiding cases and increase for opposing cases.

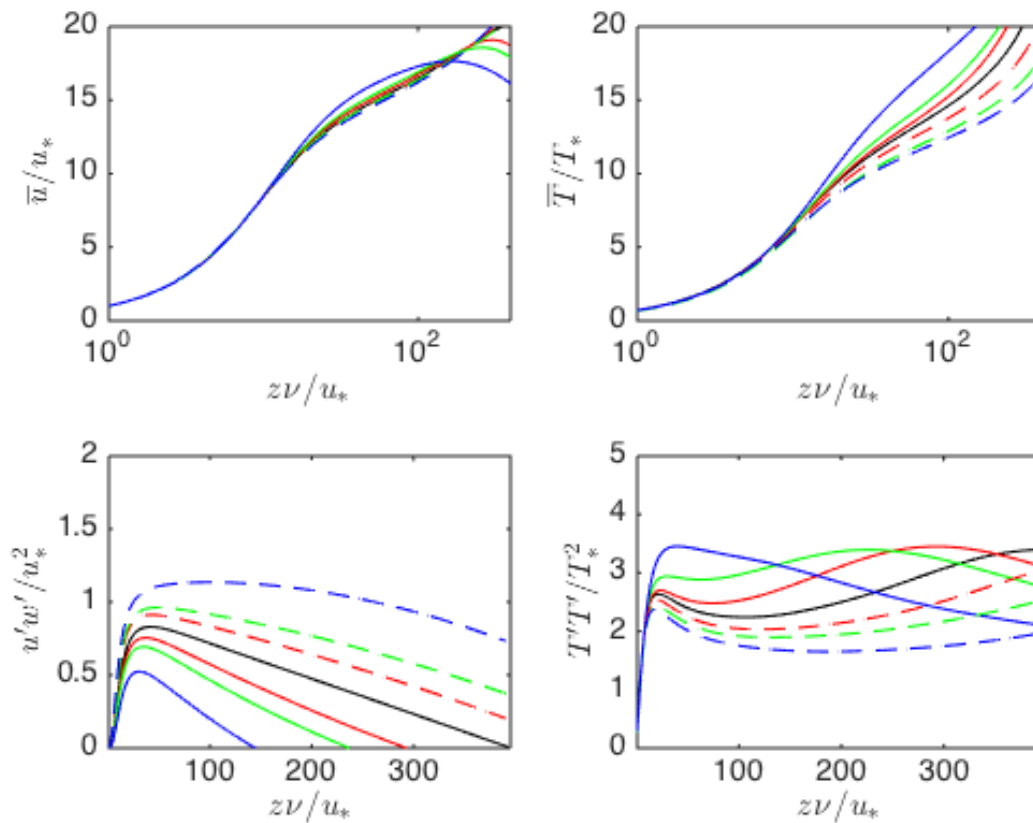


Figure 23: Mean velocity (top left) and temperature (top right) profiles of the aiding (solid line) and opposing (dashed) flows. Velocity fluctuations (Reynolds shear stress – bottom left), and temperature fluctuations (bottom right). Red  $|h/L|=0.05$ , green  $|h/L|=0.1$ , blue  $|h/L|=0.25$ , black neutral case.

## 4. Utilization Plan

The above research has enormous potential for utilization to assist emergency and disaster management organisations to predict the rate of spread and intensity of bushfires. We aim to implement these research into two broad areas:

- application models for fire behaviour analysts/regulators and
- improvements to physics based simulations.

### 4.1 Application models

#### 4.1.1. Wind reduction factor (WRF)

We aim to develop a tool (eg look –up tables or excel sheet with macros) where when ambient weather condition and vegetation condition are entered as input, it will give WRF as function of canopy height. Gradually research will be conducted to incorporate the effects of:

##### *Influence of a fire progressing under a tree canopy*

We have proposed that using an idealised model, following Harman and Finnigan (2007), for sub-canopy winds apparently predicts realistic values of wind reduction factor. This model only provides the sub-canopy winds in the absence of flame propagation. We also observed a

number of complicated flow features in our previous sub-canopy wind study, including the presence of a recirculation region at the downstream edge of the canopy. For operational forecasting it is important to understand the effect of these structures on the flame propagation. It is assumed that rate-of-spread of a fire depends only on the sub-canopy wind speed. As the fire creates a buoyant plume, which modifies the background wind profile, this assumption may not be valid and the rate-of-spread of the fire may depend on other factors such as the size of the fire.

We will be investigating the effect of the canopy and the sub-canopy winds on flame propagation under the canopy. In particular we will identify the effect of the canopy induced flow structures on the rate of fire spread and determine if the wind reduction factor depends only on the sub-canopy wind speed.

### ***Influence of atmospheric stability***

Moon, et al. [10] showed that solar radiation may have influence on the wind reduction factor and it is fairly well known that the wind velocity profile changes with the Surface temperature of the Earth. (Wyngaard [42]). However, the effect of solar radiation modifying the wind profiles in the presence of a fire may not have a significant effect on the rate of spread and other fire characteristics.

### ***Canopy inhomogeneity***

We will conduct one investigation into the effect of large scale canopy inhomogeneity on the effective roughness parameters, used in meteorological surface schemes, and on the sub-canopy wind profiles required to estimate the wind reduction factor.

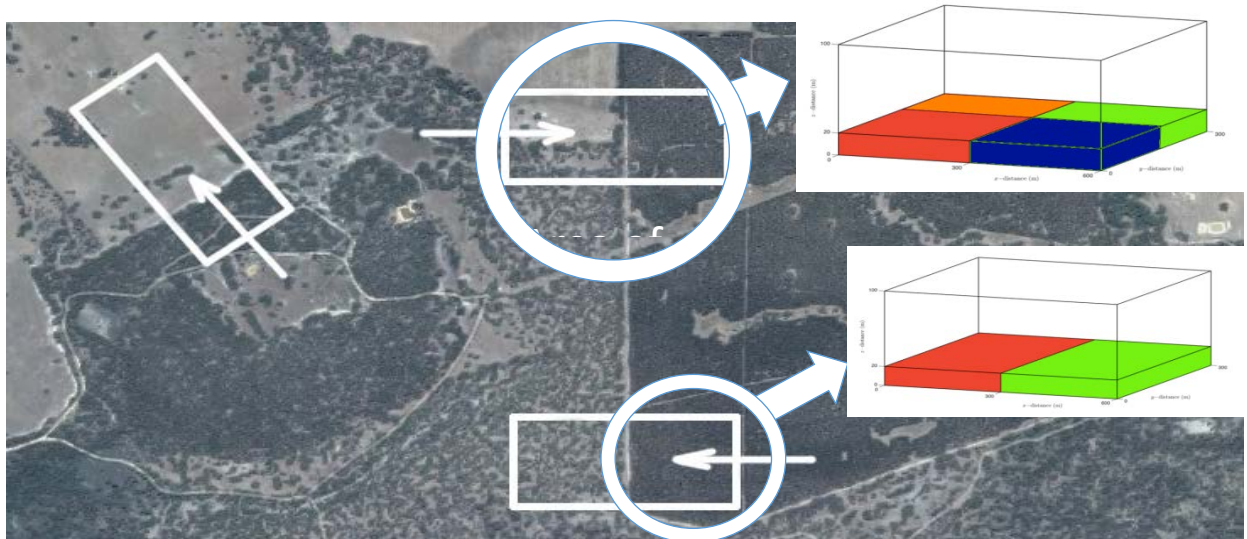


*Figure 24:Representation of in-homogeneous canopy : (below)with sparse and dense LAD (top) checker board of four different LADs.*

Because the real-world inhomogeneous forests are extremely complicated, we will initially focus on simulating idealised forests, with only one direction (that is, a strip canopy) of inhomogeneity, similar to the lower inset picture in *Figure 24*. We will then systematically

decrease the length-scale of the inhomogeneous canopies, by increasing the number of strips, to examine the effect on the flow above and within the canopy.

Canopy inhomogeneity is quite common on real world fire grounds such as shown in *Figure 24*. (The map is from a region near Ararat Victoria) The inhomogeneity can be in different directions depending on the forest and the prevailing winds. The motivation of this work is to examine the similarities (or highlight the differences) between flows through inhomogeneous forest canopies, flows through heterogeneous vegetation canopies, and flows over rough surfaces such as urban areas and hilly terrain.

### ***Terrain slope***

Combination of terrain slope and canopy may exhibit interesting physical features and significantly alter the wind profile, hence WRF. Topographical features such as upslope, downslope, crest and valley of hills can have considerable influence on WRF.

### ***Wind downstream of a canopy edge***

It is important to know how much distance wind needs to travel downstream of a canopy, before it returns to an open field wind profile. Knowledge of this redevelopment distance will help operational analysts appropriately apply wind reduction factors.

### ***WRF map***

A long term utilization goal of this project is to develop a national map of WRF. If a user clicks on a geographical location, its WRF will be shown. This work needs satellite imagery data of LAD. However we don't envisage this to be commissioned before 2025.

## **4.1.2. Statistical model for firebrand**

Once particle submodel representing firebrand transport (especially short-range spotting) is validated, the model will be used to develop correlation which takes the wind conditions, shape and mass of the firebrands as inputs and return information about the distribution of firebrand scattering, such as mean distance, width of scattering, information about ignition propensity of surface fuel. This statistical model would provide fire services some immediate support and information.

## **4.1.3 Mapping risk to WUI houses**

Physics based model equipped with validated grassfire spread and particle submodels, we can use firebrand and heat flux attack mapping on houses in the WUI. This will allow us to apprise AS3959 and subsequently attempt to incorporate firebrand attack in this standard. We can also assess:

- ignition propensity of combustibles surrounding houses
- propensity to breach envelop/house

The physics based model can be used as a tool for performance based solution to determine safe sites for infrastructure.

For grassfire propagation study will be expanded further with consideration of the effects of:

- inhomogeneous grassland (eg representing patchiness caused by grass eaten by cattle, or spinifex, gamba type grassland)
- terrain slope
- angle of wind flow
- combinations of above

This will help us to assess the RoS equations for inhomogeneous grassland and terrain slope. It is expected to improve predictions of fire behaviour made with current operational models.

#### **4.1.4 Improvement to wind-profile generating software**

An improved (by accounting for rough surfaces, tree canopies, heated earth surface etc) tool to map wind profile across the simulation domain can developed based the DNS studies based on the research presented in Section 3.5. This will generate an ideal boundary condition for any type of computer simulation. The software will include (a) quantifying effect of a single scale of boundary roughness, and (b) effect of heated earth surface on the profile of atmospheric boundary layer. This will be achieved by making an improvement to wind field generating software such as wind –ninja. The main outcome of this work will be wall-models for physics based simulation and numerical weather prediction.

#### **4.2 Improvement to physics-based modelling**

A reliable physics-based model will improve the accuracy of post-fire analysis, determination of safe sites for infrastructure, prescribed burning etc in the short term. The improved physics-based model can be coupled with high resolution weather model and LiDAR/satellite data will eventually form the next generation forecasting tool in the long term (when computer power will exponentially increase). Then it can be used for community scale fire spread prediction faster than the real time. To improve the model, we have already implemented some improvement presented in Section 2. We would like to improve the following based on the research presented in Section 3:

- Wall functions for rough surfaces, e.g. forests, houses, and undulating terrain
- Wall functions for heated vertical and inclined surface i.e. for simulating fire spread up slopes and buildings
- Improved representation of particles for firebrand simulations
- Improved filtering of LES velocity fields to ensure more accurate simulations

### **5. Conclusions**

It is essential that emergency and disaster management organisations are able to predict the rate of spread and intensity of bushfires. Currently, this is achieved by implementing simplified operational models that have the useful attribute of providing results on time scales commensurate with those required by emergency managers. However, it is essential that these non-physics-based operational tools be refined so that they can predict fire behaviour under a wide range of localised topographic and weather conditions; they also need to be able to account for a range of inhomogeneity, slope, and thermal instability within vegetation and terrain.

To help ensure that operational wildfire models are accurate and flexible, we have numerically tested and established a reliable physics-based model that is based on basic fire dynamics and corresponding differential equations to simulate bushfire scenarios. The end goal of our work

is to improve bushfire modelling so that risks and losses associated with bushfires can be reduced.

Each subproject has led to a set of conclusions which are relevant and applicable to fire spread analysis. In summary, the canopy simulations demonstrate a number of structures which may be important when calculating and applying wind reduction factors. The results of simulated grassfire show a linear dependence of rate of spread on windspeed and a systematic dependence of rate of spread on grass height (higher grassheight lower RoS) when the firefront is in the plume mode, as opposed to boundary layer mode. The firebrand generator study shows that the Lagrangian particle model, with some modification, reproduces the observed scattering distribution of the particles. We will now discuss the conclusions in greater detail.

We investigated the effect of a tree canopy on the near-surface wind speed and found that the sub-canopy winds vary with all spatial directions. In the longest canopy case (900 m long) the sub-canopy wind profile eventually becomes developed in the streamwise direction. The centre line profile of  $\bar{u}$ -velocity (streamwise) as LAD varies shows that the sub-canopy velocity profile is dominated by the drag exerted by the trunks and large branches. The drag due to the leafy crown affects the sub-canopy velocity profile significantly but only in the impact and adjustment regions at the upstream edge of the canopy. Downstream of the canopy the centre line profile of  $\bar{u}$ -velocity never completely redevelops in the domain considered here and the wake structures shed from the canopy will continue to affect any fire spread for great distances downstream.

A simple model [17] of the sub-canopy wind profile was tested. The predicted profile from physics-based modelling was found to be qualitatively correct for the most developed sub-canopy wind, though significant discrepancies exist between the model and the simulated profile in the impact and adjustment regions and above the canopy where the mean wind is still evolving to a steady profile. The simple model can be applied with very little information, namely the wind velocity far above the canopy and the LAD due to the trunks of the trees are required. The result could be used to provide an estimate of the minimum sub-canopy wind speed and hence construct an estimate of the WRF. The predicted WRF was found to be consistent with the observations of [10].

Fires in grasslands are prevalent in Australia and are relatively simple to model computationally due to the uniform fuel and flat simple terrain. We have used the CSIRO grassland experiments as validation cases for the physics-based simulations. A parametric study has been conducted where the background wind speed and the grass height was varied independently. The rate-of-spread was found to be linear with wind speed in the parameter range considered. Two simulations were conducted with different grass heights and correspondingly different bulk density, representing grass which had been cut and left on the ground. The fire in the taller grassland was found to have a higher rate-of-spread. Seven simulations were conducted where the bulk density was kept constant as height varied. In these simulations, it was observed that as the grass height increases firefront changes from boundary layer mode to plume mode. Once they are in plume mode higher grass height results in bigger fires, but slower RoS.

We are also investigating short range spotting and establishing the capability of the physics-based modelling in reliably modelling firebrand transport. A new prototype firebrand dragon is shown to successfully generate uniform showers of firebrands. The prototype is useful to study the transport dynamics of short-range firebrand transport. The Lagrangian particle model of FDS is capable of simulating the transport of non-burning solid firebrand particles with reasonable accuracy. The model is verified for two shapes of firebrand particles; the results are

somewhat under- predicted compared to experimental observations, however improvement to the results is seen with a modified drag coefficient which models the effect of particle shape. Application of the Lagrangian model for flaming firebrands will be the next step to evaluate the applicability of the model for short-range firebrand transport.

Besides the above three major aspects, we have also conducted investigations in some high impact science areas. In particular, we have focused on highly idealised direct numerical simulation of

- wind driven flow over surface roughness
- mixed convective flow over a sloped surface (flow driven by both temperature difference between surface and air and wind flow)

These works will continue as both researches as well as utilisation to improve operational models. The research will include undertaking high-level technical tasks such as implementing and validating modifications to the bushfire simulation computer code besides understanding some of the relevant physics better. Utilisation will include developing utilisation tools (tables or excel sheet), appraisal of standards, and developing easily applied approximations for fire behaviour analysts.

## 6. End-user comments

Several attempts have been made to contact end users to obtain feedback on this report and however no feedback has been received. We assume that no feedback is a consent /agreement to move forward.

## 7. References

- [1] A. L. Sullivan, "Wildland surface fire spread modelling, 1990–2007. 2: Empirical and quasi-empirical models," *International Journal of Wildland Fire*, vol. 18, pp. 369-386, 2009.
- [2] I. Noble, A. Gill, and G. Bary, "McArthur's fire-danger meters expressed as equations," *Australian Journal of Ecology*, vol. 5, pp. 201-203, 1980.
- [3] J. J. Hollis, J. S. Gould, M. G. Cruz, and W. Lachlan McCaw, "Framework for an Australian fuel classification to support bushfire management," *Australian Forestry*, vol. 78, pp. 1-17, 2015.
- [4] "AS 3959 : Construction of Buildings in Bushfire-prone Areas : Standards Australia : Sydney," 3rd Edition 2009.
- [5] G. Sanjuan, T. Margalef, and A. Cortés, "Hybrid application to accelerate wind field calculation," *Journal of Computational Science*, vol. 17, pp. 576-590, 2016.
- [6] K. McGrattan, S. Hostikka, R. McDermott, J. Floyd, C. Weinschenk, and K. Overholt, "Fire dynamics simulator, user's guide," *NIST special publication*, vol. 1019, p. 6thEdition, 2013.
- [7] W. Mell, M. A. Jenkins, J. Gould, and P. Cheney, "A physics-based approach to modelling grassland fires," *International Journal of Wildland Fire*, vol. 16, pp. 1-22, 2007.
- [8] M. Sarwar, "On linking the filter width to the boundary layer thickness in explicitly filtered large eddy simulations of wall bounded flows," *International Journal of Heat and Fluid Flow*, 2017.
- [9] E. Mueller, W. Mell, and A. Simeoni, "Large eddy simulation of forest canopy flow for wildland fire modeling," *Canadian Journal of Forest Research*, vol. 44, pp. 1534-1544, 2014.
- [10] K. Moon, T. Duff, and K. Tolhurst, "Sub-canopy forest winds: understanding wind profiles for fire behaviour simulation," *Fire Safety Journal*, 2016.
- [11] H.-B. Su, R. H. Shaw, K. T. Paw, C.-H. Moeng, and P. P. Sullivan, "Turbulent statistics of neutrally stratified flow within and above a sparse forest from large-eddy simulation and field observations," *Boundary-Layer Meteorology*, vol. 88, pp. 363-397, 1998.

- [12] B. Amiro, "Comparison of turbulence statistics within three boreal forest canopies," *Boundary-Layer Meteorology*, vol. 51, pp. 99-121, 1990.
- [13] A. Haider and O. Levenspiel, "Drag coefficient and terminal velocity of spherical and nonspherical particles," *Powder technology*, vol. 58, pp. 63-70, 1989.
- [14] A. Hölzer and M. Sommerfeld, "New simple correlation formula for the drag coefficient of non-spherical particles," *Powder Technology*, vol. 184, pp. 361-365, 2008.
- [15] K. Moinuddin and J.-d. Li, "A new convective heat transfer model for fire dynamics simulator," in *Proceedings: 13th Asian Congress of Fluid Mechanics (13 ACFM)*, 2010, pp. 819-822.
- [16] A. G. McArthur, "Fire behaviour in eucalypt forests," 1967.
- [17] I. N. Harman and J. J. Finnigan, "A simple unified theory for flow in the canopy and roughness sublayer," *Boundary-layer meteorology*, vol. 123, pp. 339-363, 2007.
- [18] N. R. Wilson and R. H. Shaw, "A higher order closure model for canopy flow," *Journal of Applied Meteorology*, vol. 16, pp. 1197-1205, 1977.
- [19] E. Inoue, "On the Turbulent Structure of Airflow within," *Journal of the Meteorological Society of Japan. Ser. II*, vol. 41, pp. 317-326, 1963.
- [20] M. Cassiani, G. Katul, and J. Albertson, "The effects of canopy leaf area index on airflow across forest edges: large-eddy simulation and analytical results," *Boundary-layer meteorology*, vol. 126, pp. 433-460, 2008.
- [21] E. Bou-Zeid, J. Overney, B. D. Rogers, and M. B. Parlange, "The effects of building representation and clustering in large-eddy simulations of flows in urban canopies," *Boundary-layer meteorology*, vol. 132, pp. 415-436, 2009.
- [22] S. B. Pope, "Turbulent flows," ed: IOP Publishing, 2001.
- [23] B. Amiro, "Drag coefficients and turbulence spectra within three boreal forest canopies," *Boundary-Layer Meteorology*, vol. 52, pp. 227-246, 1990.
- [24] S. Dupont, J.-M. Bonnefond, M. R. Irvine, E. Lamaud, and Y. Brunet, "Long-distance edge effects in a pine forest with a deep and sparse trunk space: in situ and numerical experiments," *Agricultural and Forest Meteorology*, vol. 151, pp. 328-344, 2011.
- [25] D. Morvan, S. Meradji, and W. Mell, "Interaction between head fire and backfire in grasslands," *Fire Safety Journal*, vol. 58, pp. 195-203, 2013.
- [26] E. W. Peterson and J. P. Hennessey Jr, "On the use of power laws for estimates of wind power potential," *Journal of Applied Meteorology*, vol. 17, pp. 390-394, 1978.
- [27] W. Mell, A. Maranghides, R. McDermott, and S. L. Manzello, "Numerical simulation and experiments of burning douglas fir trees," *Combustion and Flame*, vol. 156, pp. 2023-2041, 2009.
- [28] N. Cheney, J. Gould, and W. Catchpole, "The influence of fuel, weather and fire shape variables on fire-spread in grasslands," *International Journal of Wildland Fire*, vol. 3, pp. 31-44, 1993.
- [29] V. Apte, R. Bilger, A. Green, and J. Quintiere, "Wind-aided turbulent flame spread and burning over large-scale horizontal PMMA surfaces," *Combustion and Flame*, vol. 85, pp. 169-184, 1991.
- [30] K. B. McGrattan, B. Klein, S. Hostikka, and J. Floyd, "Fire Dynamics Simulator Users Guide," *NIST Special Publication 1019-5, National Institute of Standards and Technology, U.S. Department of Commerce, Gaithersburg*, 2008.
- [31] K. A. Moinuddin, K. Prasannan, R. Lalunio, and G. R. Thorpe, "Numerical Modelling of Fire Spread in Landscapes," in *8th Asia-Oceania Symposium for Fire Science and Technology* Melbourne, Australia, 2010.
- [32] G. P. Forney, "Smokeview (Version 5), A Tool for Visualizing Fire Dynamics Simulation Data, Volume II: Technical Reference Guide," *NIST Special Publication*, vol. 1017, p. 2, 2010.

- [33] S. L. Manzello, J. R. Shields, T. G. Cleary, A. Maranghides, W. E. Mell, J. C. Yang, *et al.*, "On the development and characterization of a firebrand generator," *Fire Safety Journal*, vol. 43, pp. 258-268, 2008.
- [34] S. L. Manzello and S. Suzuki, "Experimentally simulating wind driven firebrand showers in Wildland-Urban Interface (WUI) fires: overview of the NIST firebrand generator (NIST dragon) technology," *Procedia Engineering*, vol. 62, pp. 91-102, 2013.
- [35] W. Dean, "LXXII. The stream-line motion of fluid in a curved pipe (Second paper)," *The London, Edinburgh, and Dublin Philosophical Magazine and Journal of Science*, vol. 5, pp. 673-695, 1928.
- [36] K. Mohanaragam, Z. Tian, and J. Tu, "Numerical simulation of turbulent gas-particle flow in a 90° bend: Eulerian-Eulerian approach," *Computers & Chemical Engineering*, vol. 32, pp. 561-571, 2008.
- [37] R. Röhrig, S. Jakirlić, and C. Tropea, "Comparative computational study of turbulent flow in a 90 pipe elbow," *International Journal of Heat and Fluid Flow*, vol. 55, pp. 120-131, 2015.
- [38] K. Sun, L. Lu, and H. Jiang, "A computational investigation of particle distribution and deposition in a 90° bend incorporating a particle-wall model," *Building and Environment*, vol. 46, pp. 1251-1262, 2011.
- [39] K. Chu and A. Yu, "Numerical simulation of complex particle-fluid flows," *Powder Technology*, vol. 179, pp. 104-114, 2008.
- [40] M. MacDonald, L. Chan, D. Chung, N. Hutchins, and A. Ooi, "Turbulent flow over transitionally rough surfaces with varying roughness densities," *Journal of Fluid Mechanics*, vol. 804, pp. 130-161, 2016.
- [41] D. Chung, L. Chan, M. MacDonald, N. Hutchins, and A. Ooi, "A fast direct numerical simulation method for characterising hydraulic roughness," *Journal of Fluid Mechanics*, vol. 773, pp. 418-431, 2015.
- [42] J. C. Wyngaard, *Turbulence in the Atmosphere*: Cambridge University Press, 2010.